

Multiyear Mapping of Water Demand at Crop Level: An End-to-End Workflow Based on High-Resolution Crop Type Maps and Meteorological Data

Giulio Weikmann¹, Daniele Marinelli², Claudia Paris³, *Senior Member, IEEE*, Silke Migdall⁴, Eva Gleisberg, Florian Appel⁵, Heike Bach, Jim Dowling, and Lorenzo Bruzzone⁶, *Fellow, IEEE*

Abstract—This article presents a novel system that produces multiyear high-resolution irrigation water demand maps for agricultural areas, enabling a new level of detail for irrigation support for farmers and agricultural stakeholders. The system is based on a scalable distributed deep learning (DL) model trained on dense time series of Sentinel-2 images and a large training set for the first year of observation and fine tuned on new labeled data for the consecutive years. The trained models are used to generate multiyear crop type maps, which are assimilated together with the Sentinel-2 dense time series and the meteorological data into a physically based agrohydrological model to derive the irrigation water demand for different crops. To process the required large volume of multiyear Copernicus Sentinel-2 data, the software architecture of the proposed system has been built on the integration of the Food Security thematic exploitation platform (TEP) and the data-intensive artificial intelligence Hopsworks platform. While the Food Security TEP provides easy access to Sentinel-2 data and the possibility of developing processing algorithms directly in the cloud, the Hopsworks platform has been used to train DL algorithms in a distributed manner. The experimental analysis was carried out in the upper part of the Danube Basin for the years 2018, 2019, and 2020 considering 37 Sentinel-2 tiles acquired in Austria, Moravia, Hungary, Slovakia, and Germany.

Index Terms—AI4Copernicus, copernicus, deep learning (DL), Earth observation (EO), ExtremeEarth, irrigation water demand, PROMET, sustainable food production, thematic exploitation platform (TEP).

Manuscript received 2 September 2022; revised 22 February 2023, 19 June 2023, and 3 July 2023; accepted 4 July 2023. Date of publication 13 July 2023; date of current version 28 July 2023. This work was supported in part by the *ExtremeEarth* project funded by European Union's Horizon 2020 Research and Innovation Programme under Grant 825258 and in part by the *AI4Copernicus* project funded by European Union's Horizon 2020 Research and Innovation Programme under Grant 101016798. (Corresponding author: Lorenzo Bruzzone.)

Giulio Weikmann and Lorenzo Bruzzone are with the University of Trento, 38122 Trento, Italy (e-mail: giulio.weikmann@unitn.it; lorenzo.bruzzone@unitn.it).

Daniele Marinelli is with Fondazione Edmund Mach, 38098 San Michele All'Adige, Italy (e-mail: daniele.marinelli@fmach.it).

Claudia Paris is with the University of Twente, 7522 Enschede, The Netherlands (e-mail: c.paris@utwente.nl).

Silke Migdall, Eva Gleisberg, Florian Appel, and Heike Bach are with VISTA Remote Sensing in Geosciences GmbH, 80333 Munich, Germany (e-mail: migdall@vista-geo.de; gleisberg@vista-geo.de; appel@vista-geo.de; bach@vista-geo.de).

Jim Dowling is with Logical Clocks, 118 72 Stockholm, Sweden (e-mail: jim@logicalclocks.com).

Digital Object Identifier 10.1109/JSTARS.2023.3294107

I. INTRODUCTION

THE continuous acquisition of Sentinel-2¹ Copernicus data represents a unique opportunity to constantly monitor the Earth's surface at high spatial resolution. In the context of water irrigation management, Earth observation (EO) data are essential to improve water resource planning, efficient irrigation practices, monitoring of irrigation infrastructure, and early detection of droughts or floods, allowing the continuous monitoring of large-scale hydrological processes without the need of *in situ* measurements [1]. The extreme scale of such a growing volume of data requires a paradigm shift from the traditional approach of downloading, replicating, and exploiting data on local servers to a dynamic and scalable approach where the data are processed directly in the cloud. In this context, the European Space Agency (ESA) launched the thematic exploitation platforms (TEPs) in 2014 covering seven main categories: Coastal, Forestry, Geohazards, Hydrology, Polar, Urban, and Food Security. Each platform is a collaborative, virtual work environment that facilitates the access to and the exploitation of the Copernicus Big Earth observation data. Although the offered working environments provide computational resources to develop processing algorithms online, these are not sufficient for supporting cutting-edge artificial intelligence (AI) techniques aimed at advanced computing applications. In the remote sensing (RS) community, Deep learning (DL) models are more and more considered to classify effectively and efficiently continuously acquired satellite data [2], [3], [4]. The development of distributed scalable DL models requires high-performance computing platforms and GPU accelerators, which should be properly integrated with the thematic exploitation platforms (TEPs). In this context, such data and architectures can bring significant advantages to food security applications [5], [6]. These include the monitoring of agricultural areas, and in particular, the mapping of water availability and crop water demand both at field and regional scale. Indeed, in recent years, severe droughts started to hit regions typically not affected by such events, due to the lack of rain in spring/summer. The increasing spatial distribution, frequency, and severity of such events requires the monitoring of the crop water demand to mitigate the implications on

¹[Online]. Available: https://sentinels.copernicus.eu/web/sentinel/user-guides/sentinel-2-msi/document-library/-/asset_publisher/Wk0TKajiSaR/content/id/636612/S2_Products_Specification_Document

food availability and plan government interventions for new infrastructures and irrigation strategies. The production of such irrigation maps is essential not only to optimize the irrigational resources, but also to improve the crop performance, mitigate the environmental impacts, preserving the soil health, the water quality, and the ecosystem integrity. Existing methods for water demand estimation based on RS data often use hyperspectral images [7] for crop mapping. While such data provide very detailed spectral information, they lack in terms of both temporal resolution and spatial coverage. This strongly limits their use at the national or continental scale. Moreover, Sentinel-2 data are freely accessible and available, with a short revisit time of five days and spatial resolution of 10 m, making them suitable for agricultural applications at the crop field level. Hyperspectral images usually have a higher spatial resolution (30 m in average) and a smaller geometric field of view (GFOV), resulting in a wider revisit time gap. This limitation is common also to methods that use data acquired from unmanned aerial vehicle (UAV) [8]. Other methods [9] work at large scale using data acquired by low-resolution sensors such as moderate resolution imaging spectroradiometer (MODIS) thus making the field level monitoring unfeasible, as parcel sizes are often smaller than the MODIS spatial resolution.

In recent years, significant efforts have been made to link computing platforms with cloud platforms [10], [11] storing high spatial resolution EO data, to enable efficient and effective use of satellite data for specific thematic applications. In particular, the connection of such platforms is essential for the following:

- 1) access the data from various sources, removing the need to search and retrieve data manually;
- 2) process the data and perform the analysis on RS data;
- 3) customize and automate the workflows to specific thematic needs;
- 4) integrate models and algorithms;
- 5) promote collaboration and knowledge sharing among researchers and users in the RS community.

However, existing approaches are typically focused on a single-year map production and on relatively small study areas, whereas little has been done to study how to produce irrigation maps at a large scale and on a continuous basis. This article aims to address these issues by answering the following operational and interrelated research questions.

- 1) How can an end-to-end workflow be designed to effectively integrate and process satellite and meteorological data to efficiently produce irrigation maps at large scale?
- 2) How can we define a system being able to ingest the continuous stream of recently acquired satellite and meteorological data to regularly generate up-to-date irrigation maps?

To address these issues, the main novelties of this article are twofold.

- 1) To propose an end-to-end workflow that integrates the Food Security TEP and the Hopsworks platform to implement a dynamic and scalable approach where the data are processed directly in the cloud through computationally demanding DL models.

- 2) To define a novel system for producing high-resolution multiyear maps of water requirements at crop level to enable effective agricultural water management activities (i.e., continuous irrigation recommendations at crop level).

In greater detail, this article presents an efficient and effective workflow for the continuous production of high spatial resolution (10 m) annual maps for large-scale water demand assessment computed at crop level. The workflow makes extensive use of the information provided by the time series of Sentinel-2 EO data to generate continuously updated crop type maps (exploiting DL) and crop-based agrohydrological models (designed to assimilate the leaf area index (LAI) and the same Sentinel-2 EO data used for crop type mapping).

This article is organized into seven sections. Section II discusses related works. Section III presents the proposed system architecture for crop mapping and assessment of irrigation demand. Section IV describes the study area and the considered dataset. Section V illustrates the experimental results in terms of annual crop type maps (Sections V-A and V-B) and annual irrigation water demand (Sections V-C and V-D). Section VI reports the findings of the research and comments the results. Finally, Section VII concludes this article, while details of the processing architecture can be found in the Appendix.

II. RELATED WORKS

As recently remarked from the new European Green Deal [12], sustainable food production plays a central role to guarantee food security. In this context, a critical issue is the implementation of agricultural policies for an efficient and sustainable management of crops and in particular of the natural resources such as water. For the generation of field specific irrigation water demand maps, a key component is the knowledge of the planted crop types. Knowing the crop type allows the derivation of the photosynthetically active leaf area in a crop-type specific way and ultimately allows to calculate the water demand of different crops over the year [13], [14], [15]. Recently, several works have focused on the production of crop type maps on country or continental scale due to the availability of high-resolution time series of multispectral satellite data acquired with a short revisit time such as Sentinel-2 (i.e., up to 5 days) [16], [17], [18]. The temporal information allows modeling the phenological trends of different cultivation [19], which results in an accurate mapping of the crop type [20], [21]. Ibrahim et al. [16] present an automatic approach to map the main cultivation present in Nigeria based on Sentinel-2 time-series and very-high-resolution SkySat data. In [17], Sentinel-2 time series are used together with the Eurostat land use and coverage area frame survey (LUCAS) [22], [23] to generate a 10-m crop type map for the European Union (EU) for 19 crop types in 2018. Both approaches presented in [16] and [17] consider a random forest (RF) classifier, which is widely used for large-scale mapping [24]. However, Rußwurm et al. [25] compared seven deep neural networks classifiers with an RF baseline, showing that multitemporal DL approaches significantly outperform the RF

classifier for the crop type mapping problem. To emphasize the temporal information provided by the time series of Sentinel-2 images, three main categories of DL models were considered, i.e., attention-based models [26], recurrence-based models [27], and time-convolution-based models [28]. The accuracies obtained by the attention-based transformer model [29] and the recurrent models (i.e., long-short-term memory (LSTM) [30] and Star recurrent neural network (RNN) [31]) were similar, and in overall, higher compared to those of RF and time-convolution-based models [32].

In addition to the mapping of crop types, several approaches have been defined for monitoring crop water stress and assessing irrigation water demand. The latter is becoming ever more important, as water availability changes with climate change. Thus, approaches using different types of remotely sensed information are being developed. Thermal data have long been used as a basis to determine water stress. The crop water stress index, originally proposed by [33] and looking at the difference between crop canopy and ambient air temperatures, is one of the earliest examples of such indicators. More recently, this approach has been adapted so that it can be derived purely based on RS data, particularly Landsat 8 thermal data [34]. However, the bottleneck of Landsat 8 pertains to its low revisit frequency (16 daily), making it less suitable for near-real-time monitoring of crop water stress. In the absence of current high-resolution thermal missions with high revisit frequencies, researchers have looked for ways to detect crop water stress from optical imagery. Taking advantage of different portions of the electromagnetic spectrum, both multispectral and hyperspectral data are used to estimate leaf water content [35], [36], [37], [38], [39], [40], chlorophyll content [38], and xanthophyll content [38], [41] as indicators to detect water stress. Early signs of water stress are well detectable based on the near-infrared [35] or short-wave infrared part of the spectrum due to the increased reflectance near the water absorption bands or the visible (VIS) part reduced by changes in chlorophyll content [42]. Algorithms range from narrow-band spectral indices [42] over linear nonparametric regression methods such as partial least squares regressions [43], [44] to physically based radiative transfer models [36], [45], [46].

Beyond the variables that can be directly derived from EO data, additional information about the crops can be derived by crop growth modeling [47]. Using a crop growth model, soil moisture can be modeled in different soil layers and the influence of irrigation can be simulated. Thus, variables like plant water demand, water availability, and water use efficiency can be derived [48], [49]. Unlike approaches based on simple spectral indices, crop growth models allow a precise agricultural analysis at the crop level, thus enabling a better management of inputs (e.g., irrigation). However, these models are generally not used in large-scale operational workflows due to the need for crop type maps. Ensuring accurate crop type maps implies integrating DL models applied to long time series of data into the workflow, which entails the need to handle a large volume of EO data, and have high computational resources. Existing virtual work environments, which facilitate access to large volumes of data, offer limited computational resources, thus requiring to transfer large volumes of data to local servers where DL architectures

should be trained for accurate crop type mapping. Another major limitation of the literature methods is their focus on producing single year analysis. In order to monitor agricultural areas, multiyear mapping is essential to continuously provide up-to-date information. Due to both crop rotation practice and changes in the image acquisition conditions as well as the crop phenology, the class statistical distributions usually vary between years leading to a decrease of performances of a DL classifier trained on a given year when applied to a different one [50]. For this reason, it is necessary to fine tune the initial DL model on recently acquired EO data, which still requires additional computational resources.

III. PROPOSED SYSTEM FOR CROP MAPPING AND IRRIGATION DEMAND ASSESSMENT

Fig. 1 depicts the developed end-to-end work flow, which starts with the Level 1c Sentinel-2 data available on the Food Security TEP and ends with the annual irrigation water demand maps. First, the dense time series of Sentinel-2 are preprocessed in the Food Security TEP to perform the atmospheric correction, cirrus correction, cloud, and cloud shadow masking. The obtained atmospherically corrected images are further processed to generate a time series of 12 monthly composites per tile. To this end, the scalable distributed DL model is trained on the Hopsworks platform from scratch for the first year of operations, whereas it is fine tuned for the next years. The Hopsworks performs the training of the model on a parallel architecture while abstracting away the complexities of distributed computing from the user. This allows the user to focus only on the definition and configuration of the model, simplifying and accelerating the development and testing process. The trained models are then deployed on the Food Security TEP where they are used to perform the inference. In such a way, all the data processing and inference is performed on the TEP independently of the utilized model and its training. Finally, the crop type maps are provided as input together with the meteorological data and the atmospherically corrected images to the agrohydrological model employed to assess the water demand per crop field. In the following subsections, details are provided.

A. Satellite Data and Time-Series Image Preprocessing

The time series of Sentinel-2 data are the input to the production of both the crop type and the water demand maps. Starting from Sentinel-2 Level 1c data, VISTA's image processing chain implemented in the Food Security TEP performs a high-quality atmospheric correction, including high-accuracy cloud and cloud shadow masking as well as cirrus correction. After the atmospheric correction, we selected the bands having a spatial resolution of 10 and 20 m, performing a nearest neighbor interpolation on the 20-m bands to match the resolution of the highest spatial resolution channels. The atmospherically corrected data are further processed before training the DL model to harmonize the time series from the temporal view point, i.e., generate time series of uniform length across the study area. To this end, a time series of 12 monthly composites is computed per Sentinel-2 tile using a statistic-based approach working at the

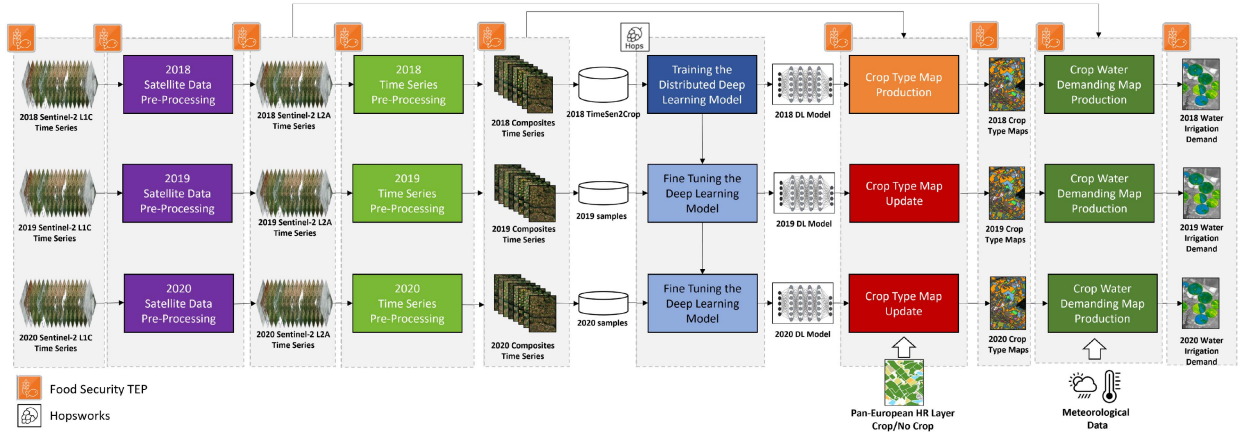


Fig. 1. End-to-end work-flow of the proposed system. While the training of the DL models requires the distributed Hopsworks platform, the other steps are processed directly in the Food Security TEP.

pixel level. Let us consider a time series of N Sentinel-2 images acquired in a given month and let us focus on one individual pixel. Let $\mathbf{X} = [\mathbf{x}_1, \mathbf{x}_2, \dots, \mathbf{x}_S]$ be the multitemporal spectral vector of the individual pixel composed by S spectral channels, where $\mathbf{x}_s = [x_s^1, x_s^2, \dots, x_s^N]$ represent the reflectance values of band s for each date, with $s \in [1, \dots, S]$. Working separately on each spectral channel, the N reflectance values are collapsed into a single one (representing the month) by computing their median. Given the median operator \mathcal{M} , the monthly composite computation for one pixel is as follows:

$$x_{c,s} = \mathcal{M} \{x_s^1, x_s^2, \dots, x_s^N\} \quad \forall s \in [1, \dots, S]. \quad (1)$$

The resulting spectral vector of the composite of one month for a pixel is $\mathbf{x}_c = [x_{c,1}, x_{c,s}, \dots, x_{c,S}]$. This operation is performed for each month and for each pixel obtaining a multitemporal spectral vector composed of $S \times 12$ features, i.e., S reflectance values for 12 months. Note that the median operator is applied after discarding cloudy, snowy, and shadowy samples using the masks provided by the atmospheric correction step. If no images are available for a given pixel for a month (e.g., due to cloud coverage), the harmonization process sets all the reflectance values of the month to zero. In this way, we ensure the uniform length of the time series. Moreover, this allows the DL model to handle the missing data by relying on the information provided by the rest of the time series [51]. Indeed, the approach is based on the assumption that a sufficient number of images is available for each month to reliably generate the composite. This assumption is reasonable due to the short revisit time of the Sentinel-2 constellation (i.e., up to 5 days). Furthermore, this step clearly mitigates the problem of missing data values in the images due to cloud cover.

B. Distributed DL Model for Crop Type Mapping

In order to accurately perform crop type classification, it is necessary to model the phenological trends of the different crops during the year [52]. To extract this information from the time series of 12 monthly composites, we considered a multitemporal DL architecture based on the LSTM architecture. This model has been selected due to its internal feedback connections, which

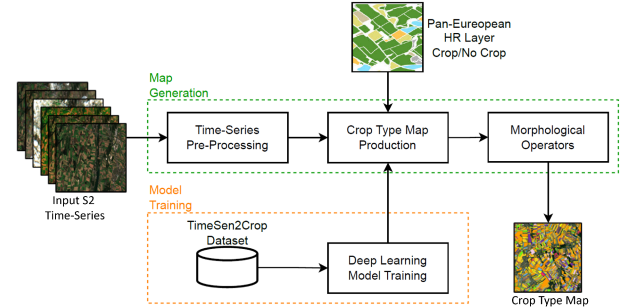


Fig. 2. Flow scheme showing the training of the LSTM model on the Hopswork platform and its use on the Food Security TEP to generate the crop type map.

are designed to model sequential data by exploiting previous observations to analyze current ones [53], [54]. Fig. 2 provides an overview of the training and classification flow for the crop type map generation, which predicts the crop type at pixel level focusing on the agricultural areas. The adopted network consists in a multilayer LSTM, where the first three layers have 200, 125, and 100 hidden units, respectively, followed by a fully connected layer and a softmax layer. The softmax layer is the one where posteriors are extracted and pixel-level classification is performed. The proposed architecture has been trained on the Hopswork platform according to a distributed strategy to distribute the workload across multiple workers each having one GPU. In this work, the architecture has been trained on two workers each having one GPU. It is worth mentioning that training the network considering two GPUs is considerably faster than training with single worker (i.e., ca. 50% of the time saved using two GPUs). However, due to the Hopswork platform, the distributed strategy can be easily scaled allowing for the use of more GPUs, further reducing the training time.

C. Crop Type Map Production and Update

After the LSTM has been trained, it is deployed on the Food Security TEP where the Sentinel-2 data are prepared to be fed to the network in the following two steps: 1) preprocessing, and

2) masking of the pixels outside agricultural areas. The first step aims to transform the time series into the format expected by the network, i.e., the 12 monthly composites, each representing a month in the selected agronomic year, according to what was presented in Section III-A. The second step aims at focusing the analysis only on agricultural areas. For this purpose, we employed the publicly available PAN-European high-resolution layer (HRL) [55], which provides information on several specific land cover characteristics at 10-m spatial resolution, including crop locations. The crop type map is generated by providing the 12 masked monthly composites to the trained network per Sentinel-2 tile to be classified. After the generation of the crop type map, few standard morphological operators are applied. This postprocessing step allows us to remove pixel-level noise leveraging the spatial correlation. In particular, an opening operation followed by an erosion using a structuring element of size 2×2 is applied to the crop type map at class level. Finally, all labeled areas smaller than a minimum threshold of 15 pixels are discarded. The filtering parameters have been defined according to the spatial resolution of the Sentinel-2 data and the minimum area of individual fields to be identified.

The architecture described so far illustrates the crop type mapping approach for the one-year scenario. However, the goal of the proposed workflow is to continuously monitor the considered agricultural area. To this end, we aim to exploit the DL model trained in 2018 to classify the new target years, i.e., 2019 and 2020, as building a new dataset for training a new model from scratch is not feasible at the operational level. However, the application of a pretrained architecture to new target years requires the definition of a domain adaptation strategy since the spectral signature changes over time and the model gradually loses its ability to correctly map crop types as the time gap between different years increases.

In order to adapt the reference year architecture to the new target years, first the irregular Sentinel-2 time series acquired in 2019 and 2020 are reprojected on the same regular time grid by exploiting the monthly composite strategy described in Section III-A. Then, the multiyear time series are harmonized in order to match the radiometric characteristics of the one used in the pretrained network, i.e., the time series of the reference year [56]. In particular, each monthly composite is initially normalized in order to have zero mean and unit variance at band level, and then, the normalized composite is processed to match the mean and the variance of the corresponding monthly composite in the reference year. Finally, we adapted the LSTM trained on 2018 considering a relatively small number of training samples for 2019 and 2020 compared to the training set used to train the architecture on the target year. These samples are used to perform the fine tuning of the pretrained network in the following two steps:

- 1) the last fully connected layer is trained, while the other layers are frozen;
- 2) the whole unfrozen network is trained considering a low learning rate.

The first step allows the network to quickly reach a convergence, while the training of the previous layers allows the optimization of computational time and avoids the divergence

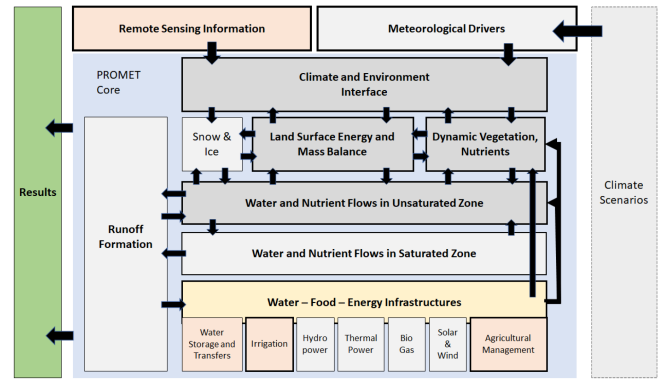


Fig. 3. Modules of the PROMET model and their connections and interfaces (modified from [58]).

from the original network [57]. By employing this approach, we can adapt the performance of the DL architecture to the new target years using a small number of training samples compared to the number of model parameters.

D. Irrigation Water Demand Map Generation

To estimate the irrigation water demand at the parcel level, the proposed end-to-end workflow leverages the well-established processes of mass and energy transfer (PROMET) model. Over the past three decades, this crop-based agrohydrological model has been employed in both scientific and service operations because of its capability of simulating all relevant energy and mass fluxes on a physical basis. Currently, this model is operationally applied to smart farming services and specifically used for irrigation advice. Moreover, the PROMET model has been designed to assimilate the LAI and the same EO data used to generate the crop type maps, thus leading to consistent output products. The main advantages of using the PROMET growth model in the considered workflow are as follows:

- 1) it allows a spatial and temporal dynamic calibration by using observed variables like measured leaf area and phenological developments [59];
- 2) it provides water recommendation at individual crop level [60];
- 3) it can model 15 different crop types [61].

Fig. 3 shows the various components of the PROMET model, which is able to integrate EO-derived land information (i.e., crop types and LAI) and meteorological data to receive an up-to-date consistency between simulated and observed variables. The crop water demand for transpiration is calculated for each hour based on the simulated potential photosynthesis. If soil moisture conditions do not suffice this water demand and irrigation is not applied, photosynthesis is reduced accordingly. As an alternative, the amount of irrigation required to avoid water stress of the crop can be calculated. Hourly values are aggregated over a longer time period (e.g., 5–7 days) and irrigation advice for the next days is provided to the farmers using meteorological forecasts in the simulations.

Fig. 4 shows the reasoning for integrating the Sentinel-2 based crop type maps and the LAI monitoring for the land

TABLE I
LIST OF DATASET USED TO PERFORM THE RESULT ASSESSMENT

Dataset	Year	Data source	Spatial resolution	Spatial coverage	Data type	Update	Result assessed
LUCAS ^a	2018	<i>in situ</i> data	1.5 m radius	Europe	CSV	Every 3 years	2018 Crop type Map
TimeSen2Crop ^b	2018	<i>in situ</i> data	10 m	Austria	CSV	-	2018 Crop type Map
Bavarian Crop Type Map ^c	2018	Farmer's declarations	Field parcel	Bavaria	Shapefile	-	2018 Crop type Map
Austrian Crop Type Map ^d	2018-2020	Farmer's declarations	Field parcel	Austria	Shapefile	Annually	2018-2020 Crop type Maps
Copernicus Climate Data Store ^e	2018-2020	Aggregation of dataset	Indicator dependant	Europe	Gridded and aggregated over shapes	Indicator dependant	2018-2020 Water Irrigation recommendations

^a <https://land.copernicus.eu/imagery-in-situ/lucas>

^b <https://rslab.disi.unitn.it/timesen2crop/>

^c <https://www.stmelf.bayern.de/index.html>

^d <https://www.data.gv.at/>

^e cds.climate.copernicus.eu/cdsapp#!/dataset/sis-energy-derived-reanalysis

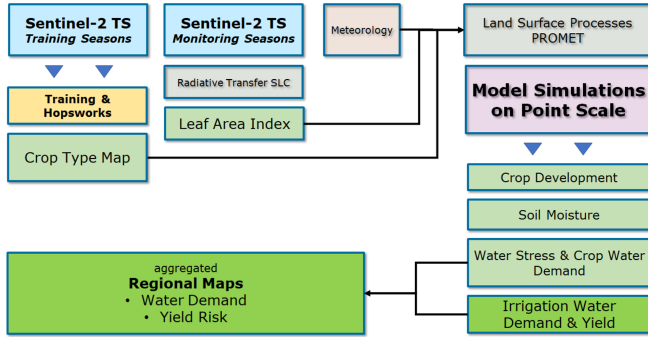


Fig. 4. Approach used based on EO and crop type maps for water demand calculations.

surface processing. Based on model simulations, all relevant crop and water information layers can be obtained and the related maps be generated. The spatial scale for the crop water demand simulations is 10×10 m, which corresponds to the spatial sampling distance of Sentinel-2. This allows us to do a direct comparison with the 10×10 m Sentinel-2 image. This means that for each sample point the crop type and the leaf area development can be derived from the corresponding Sentinel-2 pixel. The leaf area is retrieved by model inversion using the radiative transfer model soil-leaf-canopy [46] over the Sentinel-2 time series and temporally interpolated to daily values using the harmonic analysis of time series (HANTS) algorithm [62]. The leaf area information is then assimilated into the crop growth model PROMET in order to realistically simulate variables as photosynthesis and transpiration.

IV. DATASET DESCRIPTION AND EXPERIMENTAL SETUP

This section describes the considered study area, the EO and meteorological data used to perform the experimental analysis, and the validation dataset used to assess the accuracy of the obtained results summarized in Table I. Finally, details on the experimental setup are provided.

A. EO and Meteorological Data

The considered study area is covered by 37 Sentinel-2 tiles located in the Danube catchment, Europe's second largest river basin. The basin is characterized by different geographic regions ranging from the cold and humid Alps to the warm and more arid regions in the East allowing for the testing of the method under

different conditions. Three agronomic years were considered (i.e., 2018, 2019, and 2020), amounting to a total of more than 9 TB of preprocessed Sentinel-2 data made up of nine spectral bands at 10-m spatial resolution. The data available in the Food Security TEP include all the high spatial resolution spectral bands (i.e., 10 and 20 m) except for Band 8, which is discarded because of its coarser spectral resolution compared to Band 8A.

The meteorological data used in PROMET are based on downscaled model outputs from the German Weather Service German weather service (DWD). The used freely available COSMO ICON EU dataset offers hourly time steps that fit with the temporal resolution used in the PROMET model to simulate water balance components (e.g., soil moisture, surface runoff, transpiration, evaporation, and interception).

B. Validation Dataset

1) *DL Model*: To validate the crop type maps, we considered the following:

- 1) publicly available land parcel identification system (LPIS) crop type maps in Austria for the three agronomic years, which are based on farmer declarations [63];
- 2) the 2018 LUCAS database samples available for the whole study area for the 2017–2018 agronomic year;
- 3) the 2018 Bavarian crop type map, which is based on farmer declarations and available within the ExtremeEarth project provided by the Bavarian Ministry of Agriculture (“Bayrisches Staatsministerium für Ernährung, Landwirtschaft und Forsten”).

The 2018 LUCAS database and the Bavarian map are used to determine the spatial generalization capabilities of the model, i.e., in areas where no training samples are available (all Sentinel-2 tiles outside of Austria). The LUCAS database is extremely reliable since is based on *in situ* surveys collected by expert surveyors in the field. For more information, please consult Eurostat's technical reference document on the quality control procedure.² Similarly, the Bavarian map is a reliable validation source since is based on farmer declaration. The self-declaration maps follow the subsidy control in the framework of the European Common Agriculture Policy (CAP).³ Controls

²[Online]. Available: <https://ec.europa.eu/eurostat/documents/205002/8072634/LUCAS2018-C4-QCProcedures.pdf>LUCAS 2018:C4-Quality Control Procedures

³[Online]. Available: https://www.eca.europa.eu/Lists/News/NEWS1610_25/SR_LPIS_EN.pdfLand Parcel Identification System

are performed periodically to check the validity of the farmer's declarations by national or regional producer accuracy (PAs), responsible for the direct payments at a country level.⁴ These maps are considered reliable products and have been extensively used to generate training and validation dataset [25], [64], [65].

The 2019 and 2020 LPIS Austrian maps allow us to assess the generalization capability of the DL model from the temporal view point. Since the maps are used to generate the training set used for the learning of the multiyear LSTM models, we considered spatially uncorrelated portions of the study area to assess the results. This condition allows us to generate spatially uncorrelated training and test sets.

2) *PROMET Model*: To evaluate the simulation results, the PROMET model outputs are aggregated in the temporal and spatial domains. The annual maps representative of the three agronomic years are generated through integration of the simulated hourly crop water demand values. Spatially, the sample points were averaged over nomenclature of territorial units for statistics (NUTS) 1 regions, since the visualization of all sample points is not meaningful. Nevertheless, the information is generated for all of the simulated fields. To validate the observed irrigation water demand and the underlying crop water stress, we considered an indirect approach, as no large-scale in situ measurements for crop water stress or crop water demand are available for the Danube basin. Hence, the validation efforts are based on the connection between precipitation and crop water stress. We used the Copernicus Climate Data Store,⁵ aggregated to subcountry level, for our comparisons. Although no direct validation can be performed in the considered study area, we would like to remark that the PROMET model was selected for the considered end-to-end workflow since it has been extensively employed in several scientific studies [13], [47], [48], [62], [66], [67], [68], [69]. In particular, the different components of the PROMET model have been validated in order to compare simulated soil moisture profiles with measurements using time domain reflectometer (TDR) soil probes, or simulated versus measured crop parameters in terms of leaf area, biomass, crop height, and phenology. Evapotranspiration estimations were validated with Eddy covariance stations, while crop yield estimations using farm data. Several studies using PROMET can be found for EO-based LAI retrieval and data assimilation in [13], [47], and [62], for yield simulations at field scale in [48], [66], and [67], for water balance components in [68] and [69].

C. Experimental Setup

To be efficient on a large scale, the presented software architecture is based on the integration of the Food Security TEP and the data-intensive AI Hopsworks platform. While the former provides easy access to Sentinel-2 data and computational resources for processing the EO data, the latter is used

to efficiently train the developed DL models in a distributed and transparent manner. By combining the strengths of each platform, the deployed end-to-end workflow ingests the Level 1c data acquired by the Sentinel-2 satellites and provides the final products computed at large scale for multiple years.

1) *DL Model*: To successfully train the LSTM architecture on the considered study area, a large amount of high-quality informative training samples is required. As part of the *ExtremeEarth* project, we defined the TimeSen2Crop⁶ dataset [52], an open-source benchmark dataset consisting of more than one million crop type samples associated with 16 different classes. The TimeSen2Crop benchmark dataset models one agronomic year ranging from September 2017 and August 2018. The labeled samples have a minimum-distance requirement of 120 m (12 pixels) from each other, in order to reduce spatial correlation (please refer to [52] for more details on this training database). The architecture parameters were selected following a standard grid search approach, sampling the learning rate and the weight decay from log-uniform distributions, $U_{\log}([10^{-2}, 10^{-4}])$ and $U_{\log}([10^{-2}, 10^{-8}])$, respectively. We considered different numbers of cascaded layers $L \in \{2, 3, 4\}$ and hidden representation $H \in \{2^5, 2^6, 2^7\}$. The architecture has been trained on the Hopsworks platform considering synchronous distributed training on two different GPUs. For fine tuning the DL model to generate the multiyear classification, we selected 1500 samples per crop type distributed throughout the entire Austria. The seven Sentinel-2 tiles acquired in Austria were divided into minipatches, to generate training and test sets having spatially uncorrelated samples. The number of samples per crop type was defined by comparing the performance of the network without fine tuning, with 150 samples per class, and considering 1500 samples per class. The architecture performance showed limited increment after the latter, leading us to the choice of this configuration to have a good tradeoff between number of samples and performance of the architecture [56]. The accuracies of the crop type maps are reported considering the standard metrics typically used to evaluate the classification results, i.e., user accuracy (UA)%, PA%, and overall accuracy (OA)%. While the UA% measures the number of pixels correctly classified in a specific crop type with respect to the total number of pixels classified as that crop type, the PA% measures the number of pixels correctly classified in a specific crop type with respect to the total number of pixels belonging to that crop type. The OA% provides an overall assessment of the model's performance considering the accuracy of all crop types collectively. In addition, the confidence intervals are reported for all the metrics, calculated as in [70].

2) *PROMET Model*: In order to monitor crop development and irrigation water demand, a sampling approach using millions of individual fields has been chosen (see Fig. 5). Using distributed pixels reduces the number of calculations without a significant loss of local and regional heterogeneity [71]. In particular, samples are selected using a regular grid, by combining the classification result and a dynamic selection based on geometry and a quality factor. Through the applied sampling, a

⁴[Online]. Available: [https://agriculture.ec.europa.eu/common-agricultural-policy/financing-cap/assurance-and-audit/managing-payments_enIntegratedAdministrationandControlSystem\(IACS\)](https://agriculture.ec.europa.eu/common-agricultural-policy/financing-cap/assurance-and-audit/managing-payments_enIntegratedAdministrationandControlSystem(IACS))

⁵[Online]. Available: <https://cds.climate.copernicus.eu/cdsapp#!/dataset/sis-energy-derived-reanalysis>

⁶[Online]. Available: <https://rslab.disi.unitn.it/timesen2crop/>

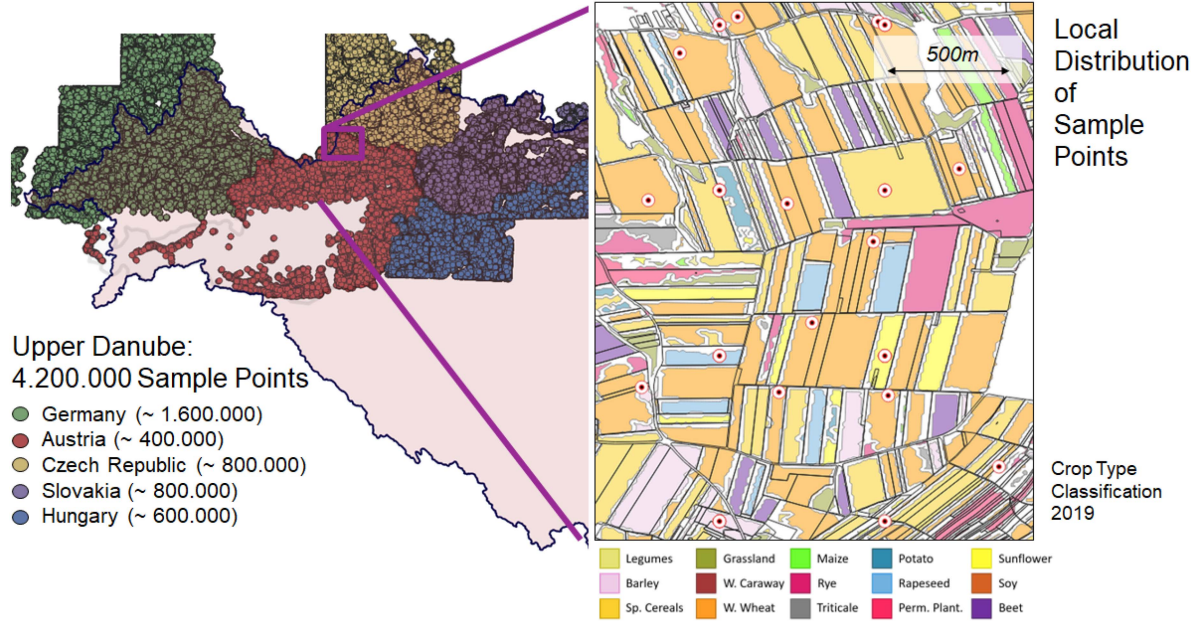


Fig. 5. Overview on the spatial setup of the PROMET simulations based on the crop type classification for the “winter wheat” crop type.

representative distribution within the administrative units considered (NUTS levels) is ensured. The crop type classification is the basis for selecting sample points that are simulated with PROMET. Samples are located at a minimum distance from field boundaries or roads to guarantee pure crop-specific remotely sensed information. Finally, more than 4 million sample points have been selected randomly distributed over all classified crop type classes in the investigated Danube basin. They cover five countries.

V. EXPERIMENTAL RESULTS

This section presents the experimental analysis carried out to assess the effectiveness of the proposed workflow. First, the spatial and temporal generalization capabilities of the DL model are assessed using the validation dataset. Then, the obtained irrigation water demand recommendations are presented at an aggregated level and crop level.

A. DL Model: Spatial Generalization Capability

To assess the spatial generalization capability of the DL model, we analyze the accuracy obtained in the entire study area. In particular, we compare the accuracy obtained in Austria (where the TimeSen2Crop training dataset is available) with the one obtained in the surrounding countries, i.e., Czech Republic, Germany, Hungary, Slovakia, and Slovenia. Due to the availability of the 2018 LUCAS in situ survey, the results reported focus on the first agronomic year (i.e., from September 2017 to August 2018). Table II shows the PA%, UA%, and OA% obtained in Austria (i.e., “Training Country”) and the rest of the study area (i.e., “Test Countries”). Please note that the results obtained per country are reported in Table V of the Appendix. The results show no noticeable drop in performance for any crop type when applying the model outside Austria, even though no

TABLE II
UA%, PA%, AND OA% CONSIDERING A 95% CONFIDENCE INTERVAL OBTAINED ON THE 2018 LUCAS IN SITU SAMPLES IN AUSTRIA WHERE TRAINING DATA WERE AVAILABLE (TRAINING COUNTRY) AND OUTSIDE AUSTRIA WHERE NO REFERENCE DATA WERE USED (TEST COUNTRIES)

Classes	Training Country		Test Countries	
	UA (%)	PA (%)	UA (%)	PA (%)
Grassland	97.22 ± 0.85	93.43 ± 1.03	94.36 ± 1.19	89.11 ± 1.20
Corn	93.72 ± 1.80	94.83 ± 1.95	97.60 ± 0.86	94.79 ± 1.46
Potato	77.08 ± 12.02	84.87 ± 10.33	73.97 ± 10.14	95.62 ± 3.89
Sunflower	96.15 ± 5.28	92.39 ± 6.08	92.50 ± 5.81	89.30 ± 6.33
Soy	88.35 ± 6.23	88.82 ± 6.24	71.21 ± 11.01	81.45 ± 10.59
Barley	72.43 ± 4.75	71.10 ± 6.46	63.38 ± 3.38	66.37 ± 4.80
Rye	48.05 ± 11.23	51.03 ± 10.39	32.00 ± 8.21	45.42 ± 9.61
Rapeseed	96.00 ± 2.91	86.34 ± 4.89	95.90 ± 1.61	91.47 ± 2.24
Beet	93.62 ± 7.06	94.38 ± 6.15	97.52 ± 2.78	88.05 ± 5.49
Winter wheat	85.63 ± 3.05	83.03 ± 2.82	87.81 ± 1.94	74.32 ± 1.79
Triticale	20.41 ± 11.40	28.61 ± 13.10	12.63 ± 4.64	48.93 ± 11.88
Perm. Plant.	48.00 ± 9.84	81.43 ± 8.05	43.54 ± 8.04	61.11 ± 7.55
OA (%)	89.10 ± 0.91		84.38 ± 0.81	

samples were used to fine tune or train the network in any of the Sentinel-2 tiles belonging to the Test Countries. In particular, the OA% obtained in Austria is 89.10%, which is comparable with the one obtained in the Test Countries, i.e., 84.38%. By analyzing the accuracy obtained for the different crop types, as expected the ones having the lowest accuracy are the following:

- 1) minoritarian classes such as “triticale” and “rye” (which are often confused, since “triticale” is a hybrid cultivation of “wheat-rye”);
- 2) mixed heterogeneous classes such as “Permanent Plantations.”

However, both UA% and PA% are above 70% for most crop types, even though a detailed classification scheme is considered compared to those used in the literature that typically have less than ten classes [25], [72].

These results are confirmed by the ones available in Table III, which shows the classification accuracies obtained

TABLE III
 QUANTITATIVE RESULTS (FOR THE 2018 AGRONOMIC YEAR) IN TERMS OF
 UA%, PA%, AND OA% CONSIDERING A 95% CONFIDENCE INTERVAL
 OBTAINED IN AUSTRIA AND BAVARIA BY THE DL MODEL TRAINED USING THE
 TIMESEN2CROP AUSTRIAN DATASET

Class	TimeSen2Crop		Bavaria	
	UA (%)	PA(%)	UA (%)	PA (%)
Legumes	87.81 ± 1.45	85.01 ± 5.55	-	-
Grassland	98.86 ± 0.19	95.56 ± 0.41	90.26 ± 0.01	97.15 ± 0.00
Corn	99.27 ± 0.14	99.74 ± 0.24	97.13 ± 0.01	92.20 ± 0.02
Potato	87.50 ± 1.00	89.29 ± 2.06	85.12 ± 0.05	71.77 ± 0.06
Sunflower	77.17 ± 5.17	83.58 ± 18.21	-	-
Soy	98.80 ± 0.21	93.57 ± 1.47	-	-
Barley	87.94 ± 0.49	98.80 ± 0.25	88.04 ± 0.02	84.60 ± 0.03
Winter caraway	96.97 ± 2.62	42.13 ± 7.32	-	-
Rye	88.60 ± 0.74	72.20 ± 1.85	55.52 ± 0.08	57.05 ± 0.06
Rapeseed	96.85 ± 0.48	98.26 ± 0.40	93.92 ± 0.02	96.52 ± 0.02
Beet	99.75 ± 0.15	97.76 ± 0.45	94.33 ± 0.02	90.31 ± 0.04
Spring cereals	95.47 ± 0.39	85.01 ± 2.86	95.51 ± 0.01	78.94 ± 0.02
Winter wheat	95.73 ± 0.32	98.88 ± 0.11	87.14 ± 0.01	90.85 ± 0.02
Triticale	76.92 ± 0.68	60.67 ± 1.61	-	-
Perm. Plant.	38.92 ± 4.97	89.84 ± 2.84	-	-
OA (%)	94.22 ± 0.25		90.71 ± 0.01	

The classification results obtained were compared with the crop type maps based on the farmer's declaration.

in 2018 considering the test set of the TimeSen2Crop dataset extracted from the Austrian crop type map based on the farmers' declarations (focusing on the Sentinel-2 tile "33UVP") and the Bavarian farmers' declarations (i.e., Sentinel-2 tiles "33UNA," "33UPA," "33UQA," "32UNV," "32UPV," "32UQV," "32UMU," "32UNU," "32UPU," "32UQU," and "33UUQ"). Similar to the results presented in Table II, the accuracy metrics are comparable for both countries. Indeed, the network achieved an OA% of 94.22% and 90.71% in Austria and Bavaria, respectively, and similar UA% and PA% in the classes present in the Bavaria region. Moreover, also in Bavaria, the "rye" class has the lowest accuracy because of its similarity with other winter cereals. A more detailed assessment can be performed in Austria due to the availability of all 15 crop types. Here, the most critical classes are "Winter Caraway" and "Permanent Plantations." The former is mainly confused with the "winter wheat" because of their similar spectral-temporal behavior. The latter is difficult to represent adequately as it is both affected by a low number of training samples (i.e., minoritarian class) and is a mixed heterogeneous class. Please note that, due to the peculiarities of the presented large-scale analysis, the availability of samples per class for different crop types varies significantly in different countries [74], [75]. Despite in the Bavaria scene only a subset of the considered classes are present in the area analyzed ("grassland," "corn," "spring cereals," "rapeseed," "potato," "rye," "sugarbeet," "barley," and "winter wheat"), the results obtained are extremely valuable since they show the generalization capacity of the network, which achieves very similar accuracy regardless of the use of training samples belonging to the Austrian country alone.

B. DL Model: Temporal Generalization Capability

To assess the temporal generalization capability of the DL model, we evaluate the accuracy of the multiyear crop type maps generated in Austria by comparing the results obtained with 2018, 2019, and 2020 farmer's based declaration LIPS

maps. Differently from Table III, the results obtained are not evaluated only in tile "33UVP" but in the whole Austrian country. However, also in this case, the validation set considered is statistical independent with respect to the training data. The multiyear classification accuracies are shown in Table IV, which compares the numerical results obtained with the fine-tuning strategy (15 000 samples for the 2019 and 2020 agronomic years) with the results obtained by using the initial DL model without any adaptation. Moreover, a comparison between the fine-tuned networks and the networks without adaptation is reported. One can observe that the fine-tuned OA% show an improvement of 7% and 5% when compared to the OA% score of the network without adaptation, for 2019 and 2020, respectively. These results demonstrate that the proposed system can be easily adapted and applied to multiyear time series for long-term monitoring analysis. Indeed, the obtained accuracies are stable in the following two agronomic years, with a small decrease in terms of performance when considering the 2020. In particular, the network achieves an OA% of 88.75% in 2018, which is comparable with 86.85% and 83.94% obtained in 2019 and 2020, respectively. The PA% and UA% values confirm these results, showing similar accuracies with the reference agronomic year. By analyzing the accuracies of different types of crops in detail, one can see that the DL model achieves stable results over time even for the most critical classes such as "triticale" and "rye" crop types. In contrast, if no fine-tuning strategy is considered, the crop type mapping accuracies decrease when the target year is far from the reference year used initially to train the architecture from scratch. Fig. 6 shows a qualitative example of crop type map obtained over the same area in the three agronomic years, i.e., 2018, 2019, and 2020. In particular, a true color representation is reported together with the multiyear maps to visually inspect the crop changes visible in the satellite data. This qualitative analysis confirms the quantitative assessment.

C. PROMET Model: Crop Level Results

Fig. 7 shows an example of simulated crop water demand estimated in 2018 and 2019 for the same crop parcels. From these qualitative results, one can notice the importance of considering a crop growth model tailored to the specific properties of different crop types. Because of the different weather patterns of 2018 and 2019, different amounts of precipitation occurred at different times of the year. The impact of such dryness was not uniform across all crops, as different crop types reacted differently to the varying weather conditions. In 2018, the dryness primarily affected "soy," causing significant challenges for their growth and yield [76]. In 2019, both "soy" and "corn" were affected, although the severity of the dry conditions on "corn" was identified as relatively milder compared to "soy." In both years, the winter crops, i.e., "winter barley" and "winter wheat," which have their main growing phase in spring, demonstrated a higher resilience to the dryness and were able to manage their water requirements more efficiently during their crucial growth stages.

Fig. 8 shows the obtained spatial irrigation recommendation generated by the PROMET model for a specific parcel. The

TABLE IV
 QUANTITATIVE RESULTS (FOR THE 2018, 2019, AND 2020 AGRONOMIC YEARS), CONSIDERING A 95% CONFIDENCE INTERVAL, IN TERMS OF UA, PA, AND OA OBTAINED BY THE ARCHITECTURES (A) TRAINED ON 2018 WITHOUT ADAPTATION ON THE 2019 AND 2020, (B) FINE TUNED ON THE 2019, AND (C) FINE TUNED ON THE 2020

Classes	Reference Year		No Adaptation				Fine Tuned Model			
	2018 (a)		2019 (a)		2020 (a)		2019 (b)		2020 (c)	
	UA (%)	PA (%)	UA (%)	PA (%)	UA (%)	PA (%)	UA (%)	PA (%)	UA (%)	PA (%)
Legumes	67.83 ± 1.77	61.45 ± 3.56	66.80 ± 1.85	55.19 ± 2.48	50.15 ± 1.89	41.98 ± 2.76	72.66 ± 1.54	76.28 ± 2.76	45.67 ± 1.54	50.72 ± 4.02
Grassland	93.87 ± 0.36	94.62 ± 0.19	80.70 ± 0.54	92.23 ± 0.47	82.41 ± 0.52	85.64 ± 0.62	96.08 ± 0.31	90.85 ± 0.33	94.85 ± 0.34	81.97 ± 0.47
Corn	91.98 ± 0.51	97.27 ± 0.28	94.84 ± 0.48	95.74 ± 0.37	88.67 ± 0.63	91.18 ± 0.64	94.65 ± 0.47	97.87 ± 0.26	93.57 ± 0.50	92.20 ± 0.54
Potato	92.64 ± 0.62	45.98 ± 1.87	67.55 ± 1.55	37.09 ± 1.63	69.58 ± 0.96	45.91 ± 1.60	79.41 ± 1.35	51.80 ± 2.09	88.06 ± 0.77	68.93 ± 1.38
Sunflower	94.26 ± 1.19	18.68 ± 1.42	55.89 ± 3.04	17.92 ± 1.31	68.29 ± 3.56	35.79 ± 1.97	62.38 ± 2.30	24.64 ± 1.67	64.21 ± 1.90	66.79 ± 3.03
Soy	67.32 ± 1.75	92.95 ± 1.34	78.04 ± 1.78	85.56 ± 1.74	43.34 ± 1.53	83.64 ± 2.06	76.55 ± 1.71	92.53 ± 1.27	67.68 ± 1.75	94.52 ± 1.08
Winter barley	89.53 ± 1.34	96.37 ± 0.55	62.00 ± 1.77	94.56 ± 1.03	63.98 ± 1.95	92.72 ± 0.67	84.95 ± 1.51	96.11 ± 0.74	75.32 ± 1.68	98.25 ± 0.39
Winter caraway	98.65 ± 0.56	16.73 ± 1.69	99.36 ± 0.72	21.79 ± 0.99	99.54 ± 0.45	33.82 ± 1.78	82.05 ± 1.60	66.30 ± 3.96	66.92 ± 1.72	85.31 ± 3.31
Rye	59.34 ± 1.85	58.74 ± 1.93	50.17 ± 2.19	32.02 ± 1.93	37.40 ± 1.46	46.00 ± 2.11	53.69 ± 1.98	40.31 ± 2.16	43.82 ± 1.59	40.55 ± 1.80
Rapeseed	95.00 ± 0.95	94.57 ± 1.61	83.81 ± 1.53	87.08 ± 2.25	97.53 ± 0.69	91.78 ± 2.05	94.39 ± 1.02	90.06 ± 1.90	89.43 ± 1.28	98.78 ± 0.65
Beet	95.09 ± 0.66	87.86 ± 2.15	84.50 ± 1.55	88.77 ± 1.76	99.31 ± 0.34	79.32 ± 1.64	88.93 ± 1.31	94.33 ± 1.27	95.94 ± 0.74	85.68 ± 1.52
Spring wheat	72.26 ± 1.04	69.54 ± 2.09	67.31 ± 1.02	71.09 ± 2.28	49.42 ± 1.09	45.35 ± 1.78	86.75 ± 0.88	72.21 ± 1.75	73.42 ± 1.10	65.81 ± 1.71
Winter wheat	89.17 ± 0.97	93.53 ± 0.52	80.19 ± 1.72	90.08 ± 0.59	96.88 ± 0.81	81.84 ± 0.63	82.31 ± 1.53	92.54 ± 0.58	90.94 ± 0.98	84.51 ± 0.70
Triticale	46.20 ± 1.81	55.58 ± 2.35	35.10 ± 1.58	42.05 ± 2.42	33.40 ± 1.63	61.81 ± 2.70	40.24 ± 1.65	45.82 ± 2.47	44.34 ± 1.78	60.60 ± 2.48
Perm plantations	74.76 ± 1.23	60.24 ± 1.71	93.06 ± 3.19	39.41 ± 1.22	85.12 ± 1.82	61.82 ± 0.96	62.64 ± 1.50	68.79 ± 2.39	66.75 ± 1.25	83.47 ± 1.15
OA(%)	88.75 ± 0.25		79.33 ± 0.38		78.41 ± 0.34		86.85 ± 0.31		83.94 ± 0.30	

Both (b) and (c) were fine tuned considering 15 000 labeled samples (1000 per Class) extracted from the year to be classified. The metrics refer to samples extracted from the one Austrian tile during the three years considered.

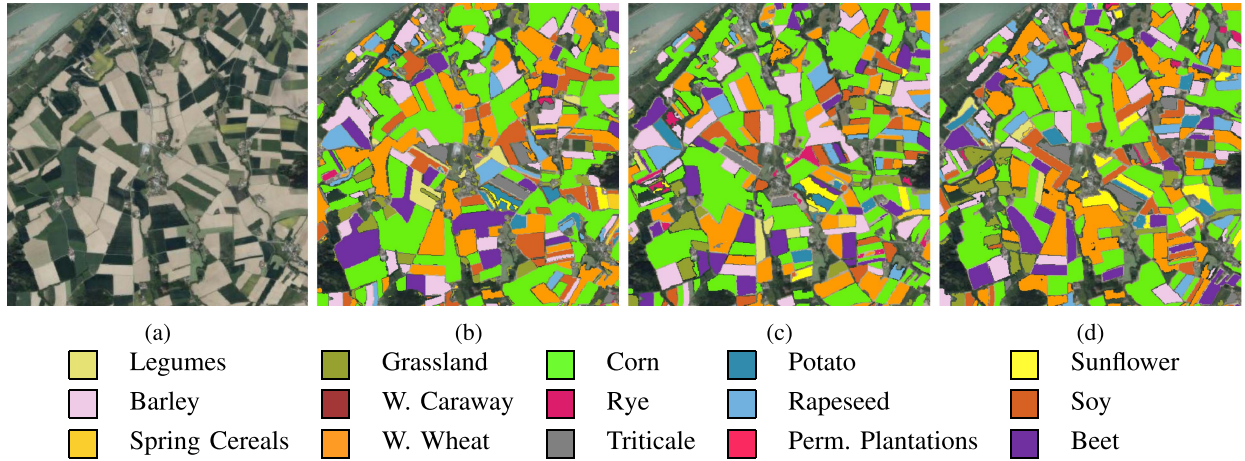


Fig. 6. Qualitative example of multiyear crop type mapping results obtained. (a) Aerial images of the patch analyzed from Environmental Systems Research Institute (ESRI) world imagery [73]. (b) 2018 crop type maps. (c) 2019 crop type maps. (d) 2020 crop type maps.

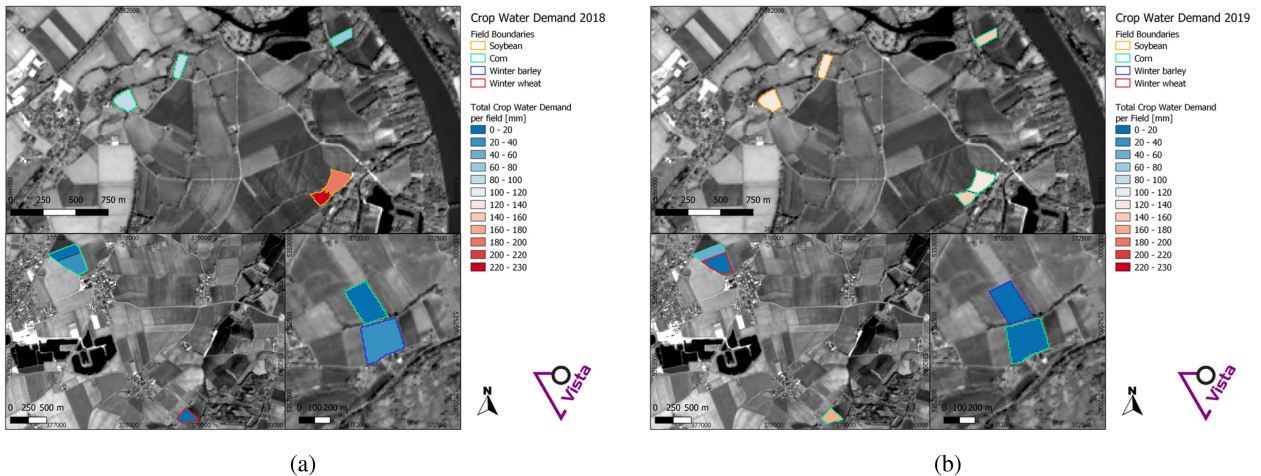


Fig. 7. Simulated irrigation water demand estimated for the same parcels in: (a) 2018 and (b) 2019.

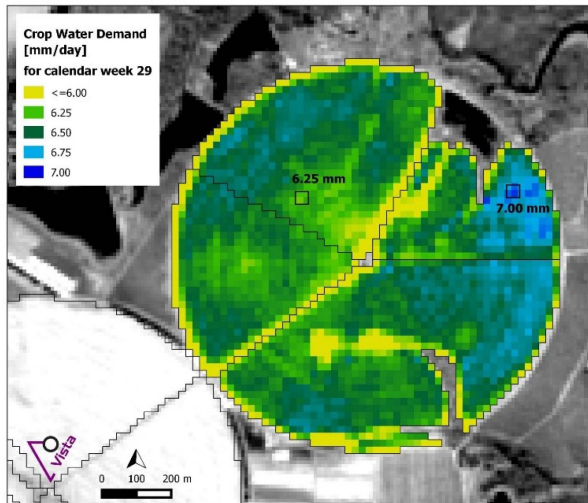


Fig. 8. Example of spatial irrigation recommendation as provided operationally to farmers using the data assimilation concept using the PROMET model and leaf area time series as retrieved from Sentinel-2.

presented example, which reports the water demand computed for week 29, highlights the spatial sensitivity of the model. Because of the model’s ability to take into account all the relevant factors that can impact irrigation (e.g., soil moisture levels, weather conditions, crop requirements, and agricultural management options like fertilization), it is possible to generate targeted recommendations at a very high spatial resolution. Within the crop, the model is able to simulate all relevant energy and mass fluxes on a physical basis at the pixel level (i.e., 10-m spatial resolution), thus leading to extremely precise crop water demand recommendations. For this reason, the PROMET model has been extensively employed in the last 30 years for smart farming services. Although this qualitative example demonstrates the capability of the PROMET model to optimize water usage and enhance crop yield at high spatial resolution, the proposed end-to-end workflow is the first attempt to perform such analysis at large scale. This is mainly due to the efficient and effective production of crop-type maps for the entire study area, which was made possible by the workflow.

D. PROMET Model: Aggregated Results

To demonstrate the effectiveness of the proposed end-to-end workflow, crop water stress and irrigation water demand were calculated using the PROMET model for the study site for the most prevalent crop types in the years between 2018 and 2020. Indeed, to the best of the author’s knowledge, no in situ data on water demand are available that cover the entirety of Austria and the area analyzed during the three selected agronomic years, making a quantitative large-scale validation not possible. However, this indirect validation performed by aggregating the results over the whole crop season and analyzing the regional differences provides a comprehensive overview at a higher level of abstraction. Fig. 9(a) shows the irrigation crop water demand for the whole season for winter wheat for the years 2018–2020. Winter wheat is harvested in July or early

August. In general, wheat does not require irrigation as can be seen in the simulations with the blue colouring. This fits with farming practice in this region. Only in the drought year 2018, some regions turn colour to red, which means that using irrigation could have increased the yield. On the contrary, as shown in Fig. 9(b), it is immediately visible that “corn” summer crop is more strongly affected by water stress and has a much higher irrigation water demand over the season. This difference is visible both in the total water demand and in the affected regions over the different years. In 2020, the total irrigation water demand was lower than in the other two years. This can be explained when looking at the precipitation variance against the 20 year mean as seen in Fig. 10. In 2020, there is overall less deviation from the mean, and especially in the third quarter of the year, (which is the summer months) more water was available than in 2018 and 2019. Nevertheless, for “corn,” there was still water stress and irrigation water demand even in 2020.

Fig. 11 shows exemplary daily modeling results for the “corn” crop type in terms of crop water stress (where 1 means no stress and lower values indicate higher water stress levels) and crop water demand (in millimeter) for two Austrian regions. For comparison, the precipitation used as modeling input is also shown in the plots. Early “corn” growth stages were not affected by water stress, but from late July through all of August, crop water demand was almost consistently higher than the available water supply, leading to water stress. In Styria, some heavier rainfalls could reduce the water stress, but they did not manage to fill the whole water demand. In order to avoid water stress for each field under investigation, the irrigation demand is simulated and displayed in the green line in Fig. 11.

VI. DISCUSSION

The objective of this article is to present a successful end-to-end workflow for the production of irrigation water demand in an operational scenario by integrating processing capabilities of the TEPs, which provides access to the Sentinel-2 data and computational resources for data processing, and the parallel computing architectures of the Hopsworks platform. By interconnecting the two infrastructures, the proposed automatic end-to-end workflow is able to process large volumes of Sentinel-2 images and provides water irrigation recommendations at crop level. This can be useful to both single farmers and stakeholders. By exploiting the Food Security TEP, the different models can be retrieved from the Hopsworks and used for the inference in a fast and effective way. This agile method allows the definition and the training of different models on the Hopsworks without the need of changing the pipeline implemented on the thematic platform. Moreover, since the TEPs allow the retrieval of different sources of data and datasets, it is possible to implement the data processing in the pipeline. One example can be found in the masking procedure of nonagricultural areas, which has to be performed before running the crop type classification. In this case, we employed the HRL map to mask the noncrop pixels. However, any other high-resolution land cover map available can be used to focus only on cultivated areas [77], [78].

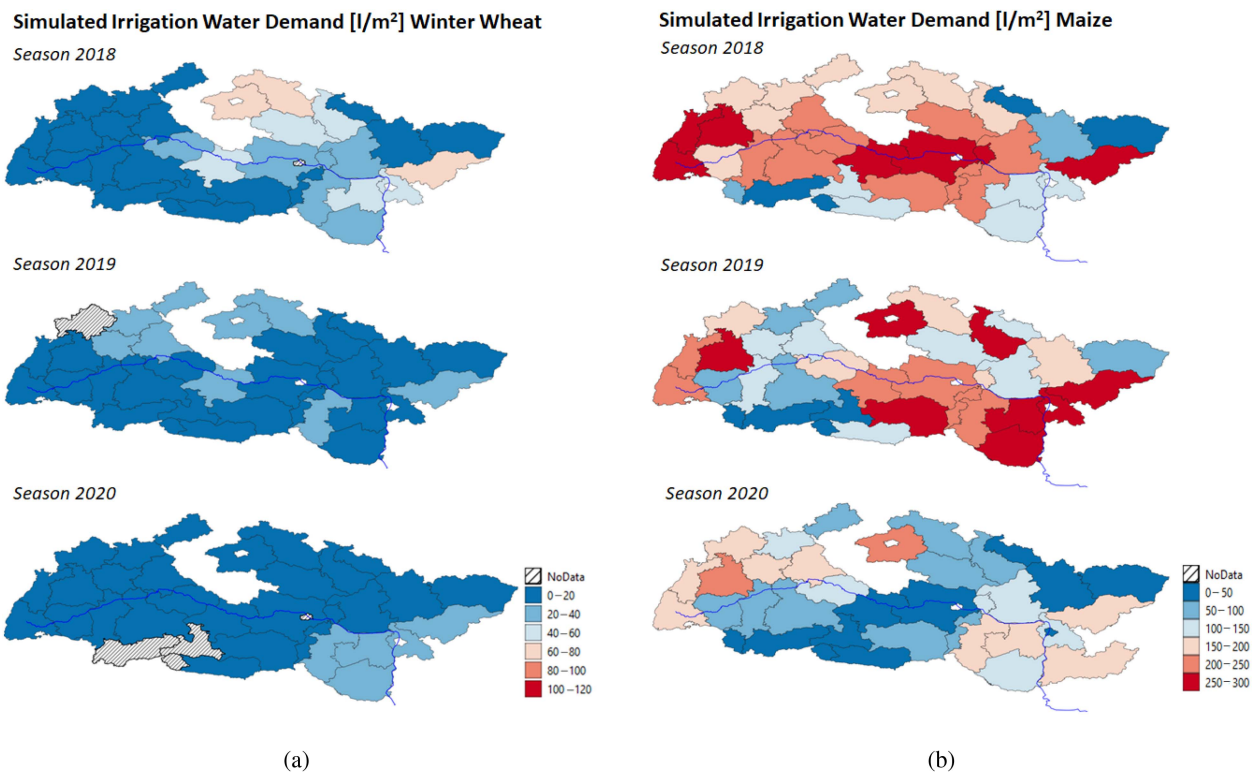


Fig. 9. Simulated irrigation water demand for the 3 considered years for: (a) “wheat,” and (b) “corn.” The results obtained are presented aggregated on NUTS 1 level and vegetation period/year.

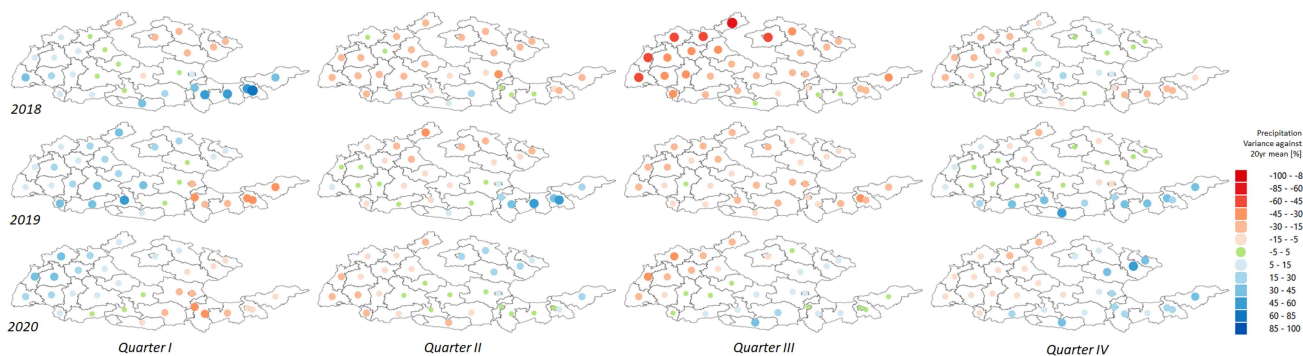


Fig. 10. Deviation of the precipitation water availability against long year statistics for the three considered years.

The LSTM DL model achieve accurate classification results from both the spatial and temporal view point. Indeed, the LSTM for 2018 obtained an OA of 85.39% and 85.20% on the LUCAS validation dataset and the farmer’s declaration map, respectively. These accuracies demonstrate that the network has good spatial generalization capability, achieving similar accuracy over the entire study area despite having been trained only on the Austrian territory. Similar results are obtained for the new target years 2019 and 2020 having an OA of 81.29% and 78.79%, respectively, considering only 15 000 training samples per year. Although the amount of labeled data used to train the network in later years is much smaller than that used to train it in 2018, the qualities of the maps obtained are visually comparable. From the qualitative example reported in Fig. 6, one can notice that the three crop type maps correctly distinguish the boundaries of

the different cultivated fields. Indeed, even though the network performs a pixel-level classification, the shape of the fields is clearly visible in the scene for all years. The results obtained confirm the effectiveness of the architecture even under conditions of multiyear maps production. Also, they accurately show the changes that have occurred on the land in different agronomic years due to crop rotation practices. Finally, we would like to emphasize that the proposed DL model can work anywhere, as long as a sufficient number of reference samples are available for training or fine tuning the DL model. It is worth noting that many efforts are currently being made to generate publicly available mapping datasets of crop types to support agricultural monitoring [72], [79]. In addition, several EU Member States are publishing agricultural information based on farmers’ declarations (collected for the monitoring of European subsidies) for research

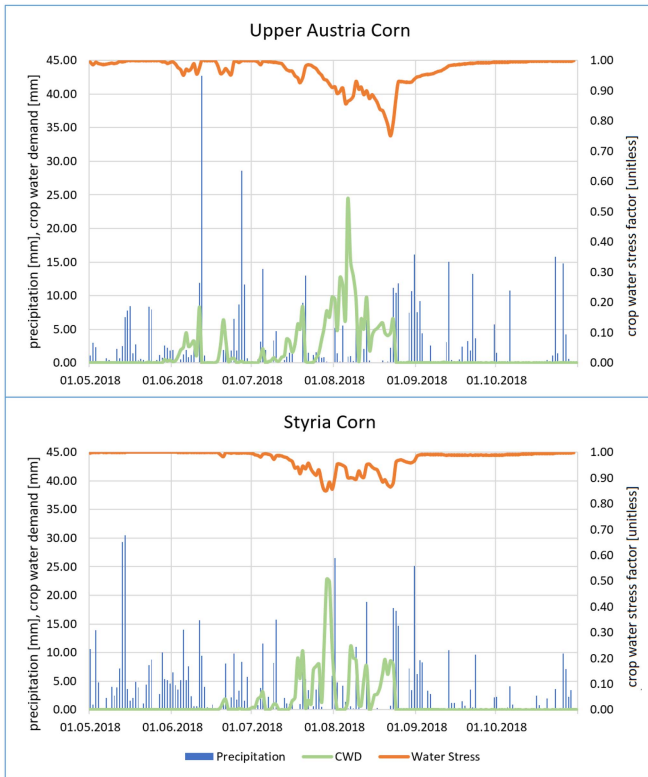


Fig. 11. Simulated crop water stress and irrigation crop water demand for “corn” for two regions in Austria in 2018.

purposes. Therefore, it is possible to conclude that the crop type mapping component of the proposed end-to-end workflow can be used to perform the continuous production of accurate crop type maps. This enables precise agricultural analysis at the crop level instead of considering basic approaches based on simple spectral indices computed for the whole study area.

The water demand assessment allowed us to infer important information about the crops under investigation. In particular, we detected a crop demand that exceeded consistently the available water supply for “corn,” leading to water stress. Examining the aggregated results over the entire crop season also allowed for an analysis of regional differences. In particular, certain crops such as “winter wheat” typically do not require irrigation, which is allineated to the farming practices in the region, but we detected a drought year in 2018 where several regions displayed red coloring, suggesting that irrigation could have increased yields. “Corn” summer crops, instead, are significantly affected by water stress [80] and require a much higher irrigation water demand throughout the season. The variance in precipitation compared to the 20-year mean also provides an explanation for the observed differences. The results demonstrate the importance of assessing crop-specific water requirements and irrigation needs based on regional and yearly variations in water availability. Understanding such dynamics can inform farmers and policymakers in implementing effective irrigation strategies and water management practices to mitigate crop water stress and optimize water use efficiency. Overall, the study conducted emphasizes the need of continuously monitoring and assessment of crop water stress

and irrigation water demand to ensure sustainable agricultural practices in the face of changing climatic conditions and water availability. Furthermore, the method suggested for choosing and combining sample points, specifically within administrative areas, involves integrating detailed data at the field level with the summarized findings at the NUTS 1 level. This approach caters to the specific requirements of individual farmers by providing operational services tailored to their needs, while also presents broader information to governmental bodies and other relevant parties. Consequently, the results can be adjusted to meet the distinct expectations of different user groups.

VII. CONCLUSION

In this article, we have presented a system for the production of multiyear water availability maps by assessment of the irrigation water demand at the crop level. We exploited time series of Sentinel-2 data for agricultural areas at 10 m of spatial resolution for wide-scale irrigation support. The end-to-end workflow was developed by integrating the Food Security TEP, which provides access to the Sentinel-2 data and computational resources for data processing, and the data-intensive AI Hopsworks platform, designed for training distributed DL models. First, the data are atmospherically corrected and preprocessed in the TEP to generate the atmospherically corrected time series of Sentinel-2 and the time series of spatially and temporally harmonized 12-month composites. Then, a scalable distributed LSTM DL model is trained on the Hopsworks platform from scratch for the first year of observation, while being fine tuned for the subsequent years. The trained models are used in the Food Security TEP to generate multiyear crop type maps, which are combined together with the meteorological data and the atmospherically corrected time series of Sentinel-2 images to assess the irrigation water demand for millions of agricultural fields by the PROMET agrohydrological model. The experimental results obtained in the upper part of the Danube Catchment for the 2018, 2019, and 2020 demonstrate the effectiveness of the proposed system.

The results obtained for crop water stress and irrigation water demand demonstrate the model’s ability to identify at which growth stages the water demand exceeds water supply. In particular, the multiyear results obtained pointed out the capability of the proposed system to capture the different levels of water stress and irrigation water demand for different crops, under different weather conditions and for different seasons. As future developments, we plan to test the proposed system architecture for multiple target years (i.e., for a 10-year window), in order to assess its robustness from the temporal view point. Moreover, we would like to test it on different countries to further evaluate its generalization capability from the spatial view point. Finally, we would like to explore the possibility of generating in-season (i.e., before the end of the year) crop type maps to be combined with short- and mid-season weather forecasts to generate predictive analyses of water stress. These early water demand forecasts can be extremely useful in providing irrigation policy advice at the local and regional levels.

APPENDIX

PROPOSED SYSTEM: PROCESSING ARCHITECTURE

The entire pipeline has been implemented on cloud computing platforms to exploit their distributed processing power and eliminate the need of downloading/uploading large amounts of data. Moreover, the use of such platforms allows for easy access to the entire processing pipeline by the service providers and final users, thus guaranteeing effective exploitation of the developed methods and generated products. According to the properties of the considered platforms, the Food Security TEP⁷ was used to implement the complete pipeline starting with the pre-processing of the Level 1c Sentinel-2 data and ending with the production of the irrigation water demand maps, whereas Hopsworks⁸ was used to specifically perform the training of the distributed DL model taking the TimeSen2Crop database as input. This condition allows us to minimize the amount of data volume transferred from one platform to the other. Indeed, to train the DL model on the Hopsworks platform, only the TimeSen2crop database has to be uploaded, without the need of transferring the whole time series of Sentinel-2 images. The obtained LSTM models can be downloaded to the TEP directly using the Hopsworks API,⁹ so that the inference procedure (i.e., production of crop type maps) can be carried out where the satellite data are available.

A. Food Security TEP Implementation

The Food Security TEP is an online platform that provides access to EO and non-EO data and the services to process them. The basic principle is to bring algorithms to the data. All the Level 1c Sentinel-2 datasets are available on the Food Security TEP via the Copernicus services within the Data and Information Access Services concept¹⁰ on the Creodias.¹¹ The Food Security TEP, operated by VISTA, holds data access mechanisms, tools for data processing and data analytics, and all solutions for scientists and service providers to process, analyze, and share data.

On the Food Security TEP, the different services components are available as processors based on docker containers associated with bash files that automatically execute the python scripts related to each particular service. Services (or processors) can be used and combined by users, according to their account level and access rights. In the considered pipeline, the steps implemented in the TEP are as follows:

- 1) the preprocessing of the Sentinel-2 data to generate the bottom-of-atmosphere images;
- 2) the preparation of the time series of 12 monthly composites per year according (see Section III-A);
- 3) the production of the multiyear crop type maps;
- 4) the crop type maps postprocessing based on morphological operators (see Section III-C).

⁷[Online]. Available: <https://foodsecurity-tep.net/>

⁸[Online]. Available: <https://www.hopsworks.ai/>

⁹[Online]. Available: <https://hops-py.logicalclocks.com/index.html>

¹⁰[Online]. Available: <https://www.copernicus.eu/en/access-data/dias>

¹¹[Online]. Available: <https://creodias.eu/>



Fig. 12. GUI of the Food Security TEP showing the service for monthly composite generation.

The final crop type maps and mechanisms are stored inside a collection in the Food Security TEP, and therefore, available to other users. Fig. 12 presents an example of the graphical user interface (GUI) of the Food Security TEP with the left part of the screen showing the service selection and setting and the right part the map over which the results are displayed.

Hopsworks is used for the distributed training of the model. It is a data-intensive platform for AI that is horizontally scalable and enables the development of end-to-end machine learning and DL pipelines. It provides the software development kit for a wide variety of operations including the following.

- 1) Machine learning feature management with a Feature Store.
- 2) Horizontally scalable distributed training on multiple machines with both CPUs and GPUs.
- 3) Model serving using Kubernetes for the deployment of the model in a container environment with Hopsworks managing secure authentication and authorization access to the model.
- 4) Model management and monitoring to manage model and experiment metadata as well as analyze the model usage in near real time.

To perform the distributed training, first the TimeSen2Crop database stored on the Hopsworks file system (HopsFS) is moved to the local machine using the Hopsworks API, and then, the temporal harmonization (see Section III-A) is applied to all the samples. Then, the distributed training of the LSTM is performed according to a multiworker mirrored strategy. In such a way, the training is performed synchronously on multiple workers, each with one GPU, by replicating the variables and computations on each device. Note that the distributed strategy can easily be scaled to run on many GPUs. From the user perspective, few modifications are required that are mostly related to enable the distributed training in the code and to define the settings of the distributed environment in the Hopsworks interface. Finally, the model is saved in HopsFS so that it can be retrieved by the Food Security TEP for the inference.

B. Extra Experimental Results

Table V reports the accuracies on the LUCAS dataset per country analyzed. Please note that some countries lack samples for all the considered classes. For both this reason and the small number of validation samples present in some countries, the

TABLE V
QUANTITATIVE RESULTS (FOR THE 2018 AGRONOMIC YEAR) IN TERMS OF UA%, PA%, AND OA% OBTAINED BY THE ARCHITECTURE ON THE LUCAS SAMPLES (DANUBE BASIN)

Class	Austria		Germany		Hungary		Czechia		Slovakia		Slovenia	
	UA (%)	PA (%)										
Grassland	97.22	93.43	95.33	88.03	91.18	93.15	91.97	84.86	95.47	93.15	99.08	96.83
Corn	93.72	94.83	97.85	95.20	96.59	90.54	99.24	95.87	96.80	93.97	94.19	98.40
Potato	77.08	84.87	76.47	85.60	-	-	71.79	99.52	-	-	-	-
Sunflower	96.15	92.39	33.33	63.66	97.18	90.21	100.00	87.18	-	-	-	-
Soy	88.35	88.82	50.00	58.62	87.50	87.21	80.00	82.95	62.50	100.00	72.73	91.31
Barley	72.43	71.10	67.82	62.05	36.23	88.84	67.74	64.19	34.04	64.33	88.89	86.41
Rye	48.05	51.03	28.89	32.86	26.67	60.06	36.07	61.26	-	-	50.00	17.66
Rapeseed	96.00	86.34	92.03	79.17	98.65	94.47	97.74	98.03	80.00	65.82	-	-
Beet	93.62	94.38	97.10	76.54	-	-	97.92	96.89	100.00	75.22	-	-
Winter wheat	85.63	83.03	79.30	73.55	91.72	75.02	95.15	77.82	66.67	79.61	75.00	88.30
Triticale	20.41	28.61	16.07	45.09	75.00	71.51	8.14	38.32	-	-	-	-
Perm. Plant.	48.00	81.43	28.00	55.82	-	-	41.38	64.17	28.57	20.82	-	-
OA (%)	89.10 ± 0.91		81.77 ± 1.41		87.13 ± 2.23		84.55 ± 1.30		87.94 ± 2.35		96.04 ± 2.19	

confidence intervals were not calculated per class but were only considered in the OA% analysis.

ACKNOWLEDGMENT

The authors would like to thank Dr. W. Angermair for granting permission to publish the results obtained from his fields.

REFERENCES

- [1] M. F. McCabe et al., "The future of Earth observation in hydrology," *Hydrol. Earth Syst. Sci.*, vol. 21, no. 7, pp. 3879–3914, 2017.
- [2] P. Ghamisi et al., "Multisource and multitemporal data fusion in remote sensing: A comprehensive review of the state of the art," *IEEE Geosci. Remote Sens. Mag.*, vol. 7, no. 1, pp. 6–39, Mar. 2019.
- [3] J. E. Ball, D. T. Anderson, and C. S. Chan, "Comprehensive survey of deep learning in remote sensing: Theories, tools, and challenges for the community," *J. Appl. Remote Sens.*, vol. 11, no. 4, pp. 042609–042609, 2017.
- [4] C. Persello et al., "Deep learning and Earth observation to support the sustainable development goals: Current approaches, open challenges, and future opportunities," *IEEE Geosci. Remote Sens. Mag.*, vol. 10, no. 2, pp. 172–200, Jun. 2022.
- [5] M. Chi, A. Plaza, J. A. Benediktsson, Z. Sun, J. Shen, and Y. Zhu, "Big data for remote sensing: Challenges and opportunities," *Proc. IEEE*, vol. 104, no. 11, pp. 2207–2219, Nov. 2016.
- [6] C. Jin et al., "Big data in food safety—A review," *Curr. Opin. Food Sci.*, vol. 36, pp. 24–32, 2020.
- [7] C. Zhang et al., "Coupling hyperspectral remote sensing data with a crop model to study winter wheat water demand," *Remote Sens.*, vol. 11, no. 14, 2019, Art. no. 1684.
- [8] A. Matese et al., "Estimation of water stress in grapevines using proximal and remote sensing methods," *Remote Sens.*, vol. 10, no. 1, 2018, Art. no. 114.
- [9] M. Romaguera, A. Y. Hoekstra, Z. Su, M. S. Krol, and M. S. Salama, "Potential of using remote sensing techniques for global assessment of water footprint of crops," *Remote Sens.*, vol. 2, no. 4, pp. 1177–1196, 2010.
- [10] M. Amani et al., "Google Earth engine cloud computing platform for remote sensing big data applications: A comprehensive review," *IEEE J. Sel. Topics Appl. Earth Observ. Remote Sens.*, vol. 13, pp. 5326–5350, Sep. 2020.
- [11] Z. Wu, J. Sun, Y. Zhang, Z. Wei, and J. Chanussot, "Recent developments in parallel and distributed computing for remotely sensed big data processing," *Proc. IEEE*, vol. 109, no. 8, pp. 1282–1305, Aug. 2021.
- [12] L. Montanarella and P. Panagos, "The relevance of sustainable soil management within the European green deal," *Land Policy*, vol. 100, 2021, Art. no. 104950.
- [13] S. Migdall, H. Bach, J. Bobert, M. Wehrhan, and W. Mauser, "Inversion of a canopy reflectance model using hyperspectral imagery for monitoring wheat growth and estimating yield," *Precis. Agriculture*, vol. 10, pp. 508–524, 2009.
- [14] P. Klug, F. Schlenz, T. Hank, S. Migdall, H. Bach, and W. Mauser, "Generating continuous information products on land use and the intensity of agricultural production from high resolution satellite data," in *Proc. IEEE Int. Geosci. Remote Sens. Symp.*, 2015, pp. 3989–3992.
- [15] S. Migdall, N. Ohl, and H. Bach, "Parameterisation of the land surface reflectance model SLC for winter rape using spaceborne hyperspectral CHRIS data," in *Proc. Hyperspectral Workshop*, 2010.
- [16] E. S. Ibrahim, P. Rufin, L. Nill, B. Kamali, C. Nendel, and P. Hostert, "Mapping crop types and cropping systems in Nigeria with Sentinel-2 imagery," *Remote Sens.*, vol. 13, no. 17, 2021, Art. no. 3523.
- [17] B. Ghassemi, A. Dujakovic, M. Žóttak, M. Immitzer, C. Atzberger, and F. Vuolo, "Designing a European-wide crop type mapping approach based on machine learning algorithms using LUCAS field survey and Sentinel-2 data," *Remote Sens.*, vol. 14, no. 3, 2022, Art. no. 541.
- [18] R. Malinowski et al., "Automated production of a land cover/use map of Europe based on Sentinel-2 imagery," *Remote Sens.*, vol. 12, no. 21, 2020, Art. no. 3523.
- [19] B. Watkins and A. Van Niekerk, "A comparison of object-based image analysis approaches for field boundary delineation using multi-temporal Sentinel-2 imagery," *Comput. Electron. Agriculture*, vol. 158, pp. 294–302, 2019.
- [20] Y. T. Solano-Correa, F. Bovolo, L. Bruzzone, and D. Fernández-Prieto, "A method for the analysis of small crop fields in Sentinel-2 dense time series," *IEEE Trans. Geosci. Remote Sens.*, vol. 58, no. 3, pp. 2150–2164, Mar. 2020.
- [21] M. Belgiu and O. Csillik, "Sentinel-2 cropland mapping using pixel-based and object-based time-weighted dynamic time warping analysis," *Remote Sens. Environ.*, vol. 204, pp. 509–523, 2018.
- [22] J. Gallego and J. Delincé, "The European land use and cover area-frame statistical survey," in *Proc. Agricultural Surv. Methods*, 2010, pp. 149–168.
- [23] Eurostat, "Land use and coverage area frame survey," Dec. 15, 2021, [Online]. Available: <https://ec.europa.eu/eurostat/web/lucas>
- [24] R. D'Andrimont, A. Verhegghen, G. Lemoine, P. Kempeneers, M. Meroni, and M. Van der Velde, "From parcel to continental scale—A first European crop type map based on Sentinel-1 and LUCAS copernicus in-situ observations," *Remote Sens. Environ.*, vol. 266, 2021, Art. no. 112708. [Online]. Available: <https://www.sciencedirect.com/science/article/pii/S0034425721004284>
- [25] M. Rußwurm, S. Lefèvre, and M. Körner, "Breizhcrocs: A satellite time series dataset for crop type identification," in *Proc. Int. Conf. Mach. Learn. Time Series Workshop*, 2019, vol. 3, pp. 1–5.
- [26] A. Vaswani et al., "Attention is all you need," in *Proc. 31st Int. Conf. Adv. Neural Inf. Process. Syst.*, 2017, vol. 30, pp. 6000–6010.
- [27] Y. Yu, X. Si, C. Hu, and J. Zhang, "A review of recurrent neural networks: LSTM cells and network architectures," *Neural Comput.*, vol. 31, no. 7, pp. 1235–1270, 2019.
- [28] H. Ismail Fawaz, G. Forestier, J. Weber, L. Idoumghar, and P.-A. Muller, "Deep learning for time series classification: A review," *Data Mining Knowl. Discov.*, vol. 33, no. 4, pp. 917–963, 2019.
- [29] M. Rußwurm and M. Körner, "Self-attention for raw optical satellite time series classification," *ISPRS J. Photogrammetry Remote Sens.*, vol. 169, pp. 421–435, 2020.

- [30] M. Rußwurm and M. Körner, "Multi-temporal land cover classification with sequential recurrent encoders," *ISPRS Int. J. Geo-Inf.*, vol. 7, no. 4, 2018, Art. no. 129.
- [31] M. O. Turkoglu, S. D'Aronco, J. Wegner, and K. Schindler, "Gating revisited: Deep multi-layer RNNs that can be trained," *IEEE Trans. Pattern Anal. Mach. Intell.*, vol. 44, no. 8, pp. 4081–4092, Aug. 2022.
- [32] C. Pelletier, G. I. Webb, and F. Petitjean, "Temporal convolutional neural network for the classification of satellite image time series," *Remote Sens.*, vol. 11, no. 5, 2019, Art. no. 523.
- [33] S. Idso, R. Jackson, P. Pinter, R. Reginato, and J. Hatfield, "Normalizing the stress-degree-day parameter for environmental variability," *Agricultural Meteorol.*, vol. 24, pp. 45–55, 1981.
- [34] S. Veysi, A. A. Naseri, S. Hamzeh, and H. Bartholomeus, "A satellite based crop water stress index for irrigation scheduling in sugarcane fields," *Agricultural Water Manage.*, vol. 189, pp. 70–86, 2017.
- [35] J. Peñuelas, I. Filella, C. Biel, L. Serrano, and R. Savé, "The reflectance at the 950–970 nm region as an indicator of plant water status," *Int. J. Remote Sens.*, vol. 14, no. 10, pp. 1887–1905, 1993.
- [36] J. Cernicharo, A. Verger, and F. Camacho, "Empirical and physical estimation of canopy water content from CHRIS/PROBA data," *Remote Sens.*, vol. 5, no. 10, pp. 5265–5284, 2013.
- [37] C. Zhang, Z. Pan, H. Dong, F. He, and X. Hu, "Remote estimation of leaf water content using spectral index derived from hyperspectral data," in *Proc. 1st Int. Conf. Inf. Sci. Electron. Technol.*, 2015, pp. 20–23.
- [38] C. Ballester et al., "Evaluating the performance of xanthophyll, chlorophyll and structure-sensitive spectral indices to detect water stress in five fruit tree species," *Precis. Agriculture*, vol. 19, no. 1, pp. 178–193, 2018.
- [39] M. Kovar, M. Brestic, O. Sytar, V. Barek, P. Hauptvogel, and M. Zivcak, "Evaluation of hyperspectral reflectance parameters to assess the leaf water content in soybean," *Water*, vol. 11, no. 3, 2019, Art. no. 443.
- [40] H. Li, W. Yang, J. Lei, J. She, and X. Zhou, "Estimation of leaf water content from hyperspectral data of different plant species by using three new spectral absorption indices," *PLoS One*, vol. 16, no. 3, 2021, Art. no. e0249351.
- [41] J. Gamon, J. Penuelas, and C. Field, "A narrow-waveband spectral index that tracks diurnal changes in photosynthetic efficiency," *Remote Sens. Environ.*, vol. 41, no. 1, pp. 35–44, 1992.
- [42] B. Bayat, C. Van der Tol, and W. Verhoef, "Remote sensing of grass response to drought stress using spectroscopic techniques and canopy reflectance model inversion," *Remote Sens.*, vol. 8, no. 7, 2016, Art. no. 557.
- [43] Y. Ge, G. Bai, V. Stoerger, and J. C. Schnable, "Temporal dynamics of maize plant growth, water use, and leaf water content using automated high throughput RGB and hyperspectral imaging," *Comput. Electron. Agriculture*, vol. 127, pp. 625–632, 2016.
- [44] A. C. Burnett, S. P. Serbin, K. J. Davidson, K. S. Ely, and A. Rogers, "Detection of the metabolic response to drought stress using hyperspectral reflectance," *J. Exp. Botany*, vol. 72, no. 18, pp. 6474–6489, 2021.
- [45] H. Bach, S. Begiebing, and W. Eder, "Analyses of CHRIS data of the aquiferex test-sites in Tunisia applying radiative transfer models," in *Proc. Envisat Symp.*, 2007.
- [46] W. Verhoef and H. Bach, "Coupled soil-leaf-canopy and atmosphere radiative transfer modeling to simulate hyperspectral multi-angular surface reflectance and TOA radiance data," *Remote Sens. Environ.*, vol. 109, no. 2, pp. 166–182, 2007.
- [47] T. B. Hank, H. Bach, and W. Mauser, "Using a remote sensing-supported hydro-agroecological model for field-scale simulation of heterogeneous crop growth and yield: Application for wheat in central Europe," *Remote Sens.*, vol. 7, no. 4, pp. 3934–3965, 2015.
- [48] E. Probst, P. Klug, W. Mauser, D. Dogaru, and T. Hank, "Water use efficiency of selected crops in the Romanian plain—model studies using Sentinel-2 satellite images," *Sci. Papers, Ser. E, Land Reclamation, Earth Observ. Surv., Environ. Eng.*, vol. 7, pp. 198–208, 2018.
- [49] S. Migdall et al., "Crop water availability mapping in the Danube basin based on deep learning, hydrological and crop growth modelling," *Eng. Proc.*, vol. 9, no. 1, 2022, Art. no. 42.
- [50] R. Sonobe, H. Tani, X. Wang, N. Kobayashi, and H. Shimamura, "Parameter tuning in the support vector machine and random forest and their performances in cross-and same-year crop classification using TerraSAR-X," *Int. J. Remote Sens.*, vol. 35, no. 23, pp. 7898–7909, 2014.
- [51] I. Podsiadlo, C. Paris, and L. Bruzzone, "A study of the robustness of the long short-term memory classifier to cloudy time series of multispectral images," *Proc. SPIE*, vol. 11533, pp. 335–343, 2020.
- [52] G. Weikmann, C. Paris, and L. Bruzzone, "TimeSen2Crop: A million labeled samples dataset of Sentinel 2 image time series for crop-type classification," *IEEE J. Sel. Topics Appl. Earth Observ. Remote Sens.*, vol. 14, pp. 4699–4708, Apr. 2021.
- [53] M. Wang, J. Wang, and L. Chen, "Mapping paddy rice using weakly supervised long short-term memory network with time series Sentinel optical and SAR images," *Agriculture*, vol. 10, no. 10, 2020, Art. no. 483.
- [54] Y. Zhou, J. Luo, L. Feng, Y. Yang, Y. Chen, and W. Wu, "Long-short-term-memory-based crop classification using high-resolution optical images and multi-temporal SAR data," *GISci. Remote Sens.*, vol. 56, no. 8, pp. 1170–1191, 2019.
- [55] Copernicus, "Pan-high resolution layers," Dec. 27, 2021. [Online]. Available: <https://land.copernicus.eu/pan-european/high-resolution-layers>
- [56] G. Weikmann, C. Paris, and L. Bruzzone, "Multi-year crop type mapping using pre-trained deep long-short term memory and Sentinel 2 image time series," *Proc. SPIE*, vol. 11862, pp. 165–175, 2021.
- [57] J. Yosinski, J. Clune, Y. Bengio, and H. Lipson, "How transferable are features in deep neural networks?," in *Proc. 27th Int. Conf. Neural Inf. Process. Syst.*, 2014, pp. 3320–3328.
- [58] T. B. Hank, "A biophysically based coupled model approach for the assessment of canopy processes under climate change conditions," Ph.D. dissertation, Faculty of Geosciences, Ludwig Maximilian Univ. Munich, Munich, Germany, 2008.
- [59] W. Mauser and H. Bach, "Promet—large scale distributed hydrological modelling to study the impact of climate change on the water flows of mountain watersheds," *J. Hydrol.*, vol. 376, no. 3/4, pp. 362–377, 2009.
- [60] U. Strasser and W. Mauser, "Modelling the spatial and temporal variations of the water balance for the Weser catchment 1965–1994," *J. Hydrol.*, vol. 254, no. 1–4, pp. 199–214, 2001.
- [61] W. Mauser et al., "Global biomass production potentials exceed expected future demand without the need for cropland expansion," *Nature Commun.*, vol. 6, no. 1, 2015, Art. no. 8946.
- [62] L. Graf, I. Kausch, H. Bach, and T. Hank, "Using harmonic analysis of green Lai time series obtained from Sentinel-2 imagery for daily representation of crop growth in a hydro-agroecological model," in *Proc. Publikationen der Deutschen Gesellschaft für Photogrammetrie, Fernerkundung und Geoinformation eV*, 2019, pp. 214–225.
- [63] AgrarMarkt Austria, "Invekos schlägt Österreich," Dec. 15, 2021. [Online]. Available: <https://www.data.gv.at/katalog/dataset/f7691988-e57c-4ee9-bbd0-e361d3811641>
- [64] D. Sykas, I. Papoutsis, and D. Zografakis, "Sen4AgriNet: A harmonized multi-country, multi-temporal benchmark dataset for agricultural Earth observation machine learning applications," in *Proc. IEEE Int. Geosci. Remote Sens. Symp.*, 2021, pp. 5830–5833.
- [65] J. Nyborg, C. Pelletier, S. Lefèvre, and I. Assent, "Timematch: Unsupervised cross-region adaptation by temporal shift estimation," *ISPRS J. Photogrammetry Remote Sens.*, vol. 188, pp. 301–313, 2022.
- [66] H. Bach and W. Mauser, "Sustainable agriculture and smart farming," in *Earth Observation Open Science and Innovation (ISSI Scientific Report Series)*, P.-P. Mathieu and C. Aubrecht, Eds. Berlin, Germany: Springer, 2018, pp. 261–269. [Online]. Available: <https://www.springer.com/us/book/9783319656328>
- [67] H. Bach, S. Migdall, F. Brohmeyer, L. Brüggemann, and M. Buddeberg, "Satellitengestützte Ertragsserhebung," *Schriftenreihe des LfULG, Heft 21/2016*; Herausgeber: Landesamt für Umwelt, Landwirtschaft und Geologie, Sachsen, no. 21, pp. 1–85, 2016. [Online]. Available: <https://publikationen.sachsen.de/bdb/artikel/13631>
- [68] W. Mauser et al., "Virtual water values—A project for global and regional assessment of agricultural yields and water use efficiency," *Sci. Papers, Ser. E, Land Reclamation, Earth Observ. Surv., Environ. Eng.*, vol. 7, pp. 192–197, 2018.
- [69] T. Hank et al., "Using Copernicus data and growth modelling to globally assess virtual water flows in agricultural production—the ViW a concept," in *Proc. IEEE Int. Geosci. Remote Sens. Symp.*, 2018, pp. 9086–9089.
- [70] P. Olofsson, G. M. Foody, M. Herold, S. V. Stehman, C. E. Woodcock, and M. A. Wulder, "Good practices for estimating area and assessing accuracy of land change," *Remote Sens. Environ.*, vol. 148, pp. 42–57, 2014. [Online]. Available: <https://www.sciencedirect.com/science/article/pii/S0034425714000704>
- [71] A. Becker and P. Braun, "Disaggregation, aggregation and spatial scaling in hydrological modelling," *J. Hydrol.*, vol. 217, no. 3/4, pp. 239–252, 1999.

- [72] G. Tseng, I. Zvonkov, C. L. Nakalembe, and H. Kerner, "Cropharvest: A global dataset for crop-type classification," in *Proc. 35th Conf. Neural Inf. Process. Syst. Datasets Benchmarks Track (Round 2)*, 2021, pp. 1–14.
- [73] *Esri World Imagery*, ArcGIS, Jun. 8, 2023. [Online]. Available: <https://www.arcgis.com/home/item.html?id=10df2279f9684e4a9f6a7f08febac2a9>
- [74] O. Erenstein, J. Chamberlin, and K. Sonder, "Estimating the global number and distribution of maize and wheat farms," *Glob. Food Secur.*, vol. 30, 2021, Art. no. 100558.
- [75] R. D'Andrimont, A. Verhegghen, G. Lemoine, P. Kempeneers, M. Meroni, and M. Van der Velde, "From parcel to continental scale—A first European crop type map based on Sentinel-1 and LUCAS copernicus in-situ observations," *Remote Sens. Environ.*, vol. 266, 2021, Art. no. 112708.
- [76] *Crop Production in EU Standard Humidity by NUTS 2 Regions*, Eurostat, Jul. 1, 2023. [Online]. Available: https://ec.europa.eu/eurostat/web/products-datasets/-/apro_cpshr
- [77] F. Chaaban, J. El Khattabi, and H. Darwishe, "Accuracy assessment of ESA worldcover 2020 and ESRI 2020 land cover maps for a region in Syria," *J. Geovisualization Spatial Anal.*, vol. 6, no. 2, 2022, Art. no. 31.
- [78] C. F. Brown et al., "Dynamic world, near real-time global 10 m land use land cover mapping," *Sci. Data*, vol. 9, no. 1, 2022, Art. no. 251.
- [79] M. Schneider, A. Broszeit, and M. Körner, "EuroCrops: A PAN-European dataset for time series crop type classification," in *Proc. Conf. Big Data Space*, 2021, pp. 125–128.
- [80] M. M. Chaves, J. P. Maroco, and J. S. Pereira, "Understanding plant responses to drought—from genes to the whole plant," *Funct. Plant Biol.*, vol. 30, no. 3, pp. 239–264, 2003.



Giulio Weikmann received the "Laurea" (B.S.) and the "Laurea Specialistica" (M.S.) (summa cum laude) degrees in information and communication engineering, in 2018 and 2020, respectively, from the University of Trento, Trento, Italy, where he is currently working toward the Ph.D. degree in information and communication technology with the Remote Sensing Laboratory (RSLab).

He has been a Teaching Assistant with the Department of Information Engineering and Computer Science, University of Trento, since 2020. He conducts

research within the frameworks of national and international projects on the topics of his research interests, which include image and signal processing and the development of deep learning architectures for the automatic processing and classification of remote sensed optical data.

Mr. Weikmann was the recipient of the Prize for the 2022 Eugenio Zilioli Best Italian Master Thesis in remote sensing, awarded by the Italian Association for Remote Sensing and the National Research Council of Italy (CNR-IREA).



Daniele Marinelli received the "Laurea" (B.Sc.) degree in electronics and telecommunications engineering, the "Laurea Magistrale" (M.Sc.) degree in telecommunications engineering (cum laude), and the Ph.D. degree in information and communication technologies (cum laude), all from the University of Trento, Trento, Italy, in 2013, 2015, and 2019, respectively.

From 2017 to 2022, he was a Teaching Assistant at the Department of Information Engineering and Computer Science, University of Trento. In 2017, he

was a Visiting Ph.D. Student at the Integrated Remote Sensing Studio, University of British Columbia, Vancouver, BC, Canada, working on Change Detection in LiDAR data for forestry applications. He is currently a Researcher with the Forest Ecology Unit of Fondazione Edmund Mach, San Michele All'Adige, Italy. His research interests include the multitemporal analysis of Hyperspectral, LiDAR data, and optical time series for forest monitoring.

Dr. Marinelli was the recipient of the prizes for the 2020 Best Italian Ph.D. Thesis and 2015 Best Italian Master Thesis in the area of remote sensing awarded by the Italy Chapter of the IEEE Geoscience and Remote Sensing Society. He got Second Place in the Student Paper Competition at the 2018 IEEE International Geoscience and Remote Sensing Symposium, Valencia, Spain.



Claudia Paris (Senior Member, IEEE) received the "Laurea" (B.S.), "Laurea Specialistica" (M.S.) (summa cum laude) degrees in telecommunication engineering and the Ph.D. degree in information and communication technology, all from the University of Trento, Trento, Italy, in 2010, 2012, and 2016, respectively.

She accomplished the Honors Master Program in Research within the Master's degree in telecommunication engineering in 2012. In 2014, she was a visiting Ph.D. student at the Rochester Institute of Technology (RIT), Rochester, NY, USA, working on the fusion of airborne and terrestrial LiDAR data. In 2016, she was a visiting Postdoc at the Instituto Superior Técnico, Lisbon, Portugal, working on the super-resolution of multiresolution multispectral remote sensing images. She is currently an Assistant Professor with the Faculty of Geo-Information Science and Earth Observation (ITC), University of Twente, Enschede, The Netherlands. She is specialized in the classification and fusion of multisource remote sensing data (e.g., LiDAR, hyperspectral, multispectral, and high-resolution optical images), multitemporal image analysis, domain-adaptation methods, developing *ad hoc* deep learning solutions, and biophysical parameter estimation. She focuses on passive and active remote sensing and aims to develop innovative and automatic techniques for large-scale environmental monitoring. Her research interests include various areas such as remote sensing image processing, signal processing, pattern recognition, image processing, machine learning, and deep learning, specifically applied to remote sensing image analysis.

Dr. Paris has been a member of the Scientific Committee and of the Technical Program Committee of the IEEE International Geoscience and Remote Sensing Symposium (IGARSS) since 2020. Since 2019, she has been a Member of the Programme Committee of the International SPIE Symposium on Remote Sensing. She is a Reviewer for many international journals and she is an Associate Editor for the IEEE GEOSCIENCE AND REMOTE SENSING LETTERS. She was twice the recipient of the prestigious Symposium Prize Paper Award (exceptional paper in terms of content and impact on the Geoscience and Remote Sensing Society) at the 2016 IEEE IGARSS (Beijing, China, 2016) and at the 2017 IEEE IGARSS (Fort Worth, TX, USA, 2017).



Silke Migdall received the Diploma degree in physical geography (equivalent to M.Sc.) from the Ludwig-Maximilians-University of Munich, Munich, Germany, in 2005.

She has almost 20 years of experience in the monitoring of agricultural crops using optical satellite imagery and model-based analyses approaches. She has been a Project Manager of many international studies. She is currently a Managing Director with Vista GmbH, Munich, Germany. Her research interests include radiative transfer modeling for derivation

of biophysical plant parameters, and the development and application of multi- and hyperspectral data analysis methods.



Eva Gleisberg received the M.Sc. degree in climate and environment sciences with a focus on remote sensing, from the Universität of Augsburg, Augsburg, Germany, in 2018.

She has worked on yield modeling of different crop types in Germany based on Sentinel-2 data in combination with the crop growth model PROMET. She is experienced in analyzing both optical satellite data. In the ExtremeEarth project, she was calculating yield and water demand for the upper Danube River basin. She is experienced with site-specific as well as large-scale analyses of satellite data for agriculture. She is working as a Project Scientist with Vista GmbH, Munich, Germany. At Vista, she works in quality control as well as in the further development and optimization of the processes of TalkingFields products and services.



Florian Appel received the Diploma degree in physical geography (equivalent to M.Sc.) from the Ludwig-Maximilians-University of Munich, Munich, Germany, in 2000.

He joined VISTA GmbH, Munich, in 2000, where he gained interest, experience, and expertise in Earth observation (EO) and data processing. He gathered experience in application development, data analytics, programming of service chains, and business applications (services, data portals, computing, and consultancy). His research interests include combin-

ing EO data, operational processing with additional data sources (in-situ / GNSS) and application of sophisticated and artificial intelligence approaches, cloud computing, and data forecasts.

Mr. Appel participated in national and international service projects and in commercial services in the EO service domain. He was active in the management of the Food Security TEP and the Innovation and Exploitation Management of Extreme Earth. He was involved as a Member of the Board of Directors of Polar View Earth Observation Limited (UK / CA / DK) (2012–2021) and a Member of the Jury of Copernicus Masters (2018–2022).



Heike Bach received the diploma degree in hydrology from the University of Freiburg, Freiburg, Germany, in 1990, and the Ph.D. degree in physical geography (Doctor rerum naturalium) from the University of Munich, Munich, Germany, in 1995.

Since 1995, she is the Founder and the CEO of VISTA, Munich, an innovative company specialized in applications of remote sensing in hydrology and agriculture. In 2017, she successfully transferred the SME into a company belonging to the BayWa Group.

Bringing scientifically sound solutions into practice in order to solve societal challenges is her strong motivation and passion. For example, VISTA's Smart Farming solutions (TalkingFields) are applied now in more than 20 countries outside Europe. The core applications include site-specific fertilisation, irrigation management, and yield forecasting. VISTA uses the opportunities of digitalization, big data, environmental models, and satellite image analyses to support sustainable agriculture and water management.



Jim Dowling received the Ph.D. degree in distributed systems from Trinity College Dublin, Dublin, Ireland, in 2005.

He has worked with MySQL AB, Cupertino, CA, USA. He is currently the CEO of Logical Clocks, Stockholm, Sweden, and an Associate Professor with the KTH Royal Institute of Technology, Stockholm. He is the Lead Architect of the open-source Hopworks platform, a horizontally scalable data platform for machine learning that includes the industry's first Feature Store. He is a Distributed Systems

Researcher. His research interests include large-scale distributed systems and machine learning.



Lorenzo Bruzzone (Fellow, IEEE) received the Laurea (M.S.) degree in electronic engineering (summa cum laude) and the Ph.D. degree in telecommunications from the University of Genoa, Genoa, Italy, in 1993 and 1998, respectively.

He is currently a Full Professor of telecommunications with the University of Trento, Trento, Italy, where he teaches remote sensing, radar, and digital communications. He is also the Founder and the Director of the Remote Sensing Laboratory (<https://rslab.disi.unitn.it/>), Department of Information Engineering and Computer Science, University of Trento. He is the Principal Investigator of many research projects. Among the others, he is currently the Principal Investigator of the Radar for Icy Moon Exploration (RIME) instrument in the framework of the Jupiter ICy moons Explorer (JUICE) mission of the European Space Agency (ESA) and the Science Lead for the High Resolution Land Cover project in the framework of the Climate Change Initiative of ESA. He is the author (or co-author) of 294 scientific publications in referred international journals (221 in IEEE journals), more than 340 papers in conference proceedings, and 22 book chapters. He is editor or co-editor of 18 books/conference proceedings and one scientific book. His papers are highly cited, as proven from the total number of citations (more than 44 000) and the value of the h-index (99) (source: Google Scholar). He promotes and supervises research on the topics of his research interests within the frameworks of many national and international projects, which include the areas of remote sensing, radar and synthetic aperture radar, signal processing, machine learning, and pattern recognition.

Dr. Bruzzone was invited as a keynote speaker in more than 40 international conferences and workshops. Since 2009, he has been a Member of the Administrative Committee of the IEEE Geoscience and Remote Sensing Society (GRSS), where since 2019, he has been the Vice-President for Professional Activities. He ranked first in the Student Prize Paper Competition of the IEEE International Geoscience and Remote Sensing Symposium (IGARSS), Seattle, WA, USA, in 1998. Since then, he has been the recipient of many international and national honors and awards, including IEEE GRSS 2015 Outstanding Service Award, the 2017 and 2018 IEEE IGARSS Symposium Prize Paper Awards, and the 2019 WHISPER Outstanding Paper Award. He was a Guest Co-Editor of many Special Issues of international journals. He is the Co-founder of the IEEE International Workshop on the Analysis of Multi-Temporal Remote-Sensing Images (MultiTemp) series and is currently a member of the Permanent Steering Committee of this series of workshops. Since 2003, he has been the Chair of the SPIE Conference on Image and Signal Processing for Remote Sensing. He has been the founder of the IEEE GEOSCIENCE AND REMOTE SENSING MAGAZINE for which he was the Editor-in-Chief between 2013 and 2017. He was a Distinguished Speaker of the IEEE Geoscience and Remote Sensing Society between 2012 and 2016. He is currently an Associate Editor for the IEEE TRANSACTIONS ON GEOSCIENCE AND REMOTE SENSING.